The physical and chemical evolution of low-salinity magmatic fluids at the porphyry to epithermal transition

A thermodynamic study

Journal Article

Author(s):
Heinrich, Christoph A.

Publication date:
2005

Permanent link:
https://doi.org/10.3929/ethz-b-000053058

Originally published in:
Mineralium Deposita 39(8), https://doi.org/10.1007/s00126-004-0461-9

Mineralium Deposita (2005) 39: 864–889
DOI 10.1007/s00126-004-0461-9

ARTICLE

Christoph A. Heinrich

The physical and chemical evolution of low-salinity magmatic fluids at the porphyry to epithermal transition: a thermodynamic study

Received: 20 February 2004 / Accepted: 4 December 2004 / Published online: 9 February 2005

Abstract Fluid-phase relationships and thermodynamic reaction modelling based on published mineral solubility data are used to re-assess the Cu–Au-mineralising fluid processes related to calc-alkaline magmatism. Fluid inclusion microanalyses of porphyry ore samples have shown that vapour-like fluids of low to intermediate salinity and density (~2–10 wt% NaCl eq.; ~0.1–0.3 g cm^{-3}) can carry percentage-level concentrations of copper and several ppm gold at high temperature and pressure. In epithermal deposits, aqueous fluids of similar low to intermediate salinity but liquid-like density are ubiquitous and commonly show a magmatic isotope signature. This paper explores the physical evolution of low-salinity to medium-salinity magmatic fluids of variable density, en route from their magmatic source through the porphyry regime to the near-surface epithermal environment, and investigates the chemical conditions required for effective transport of gold and other components from the magmatic to the epithermal domain. Multicomponent reaction modelling guided by observations of alteration zonation and vein overprinting relationships predicts that epithermal gold deposits are formed most efficiently by a specific succession of processes during the evolution of a gradually cooling magmatic–hydrothermal system. (1) The low-salinity to medium-salinity fluid, after separating from the magma and possibly condensing out some hypersaline liquid in the high-temperature porphyry environment, must physically separate from the denser and more viscous liquid, and then cool within the single-phase fluid stability field. By cooling under adequate confining pressure, such a vapour will evolve above the critical curve and contract, without any heterogeneous phase change, to an aqueous liquid of the same salinity. (2) High concentrations of gold, transported as stable Au bisulphide complexes supporting > 1 ppm Au even at 200°C, can be maintained throughout cooling, provided that the fluid initially carries an excess of H_2S over Cu + Fe on a molal scale. This condition is favoured by an initially high sulphide content in a particularly low-salinity magmatic fluid, or by preferential partitioning of sulphur into a low-salinity vapour and partial removal of Fe into a hypersaline liquid at high temperature. (3) Acid neutralisation further optimises gold transport by maximising the concentration of the HS^- ligand. This may occur by feldspar destructive alteration along pyrite ± chalcopyrite ± sulphate veins, in the transition zone between the porphyry and epithermal environments. An alternative acid/base control is the dissolution of calcite in sediments, which may enable long-distance gold transport to Carlin-type deposits, because of the positive feedback between acid neutralisation and permeability generation. The three physical and chemical transport requirements for high-grade epithermal gold mineralisation are suggested to be the common link of epithermal gold deposits to underlying magmatic–hydrothermal systems, including porphyry-Cu–Au deposits. Both mineralisation types are the result of gradual retraction of isotherms around cooling hydrous plutons in similar tectonic and hydrologic environments. As magmatic fluid is generated at increasing depths below the surface the importance of vapour contraction increases, leading to the typical overprinting of potassic, phyllic and advanced argillic alteration and their related ore styles.

Keywords Gold · Copper · Arsenic solubility · Magmatic fluids · Vapour contraction · Hypersaline liquid · Condensation · Epithermal · Porphyry · Thermodynamic modelling

Editorial handling: B. Lehmann

C. A. Heinrich (✉)
Isotope Geochemistry and Mineral Resources,
Department of Earth Sciences,
Swiss Federal Institute of Technology,
ETH Zentrum NO, 8092 Zürich, Switzerland
E-mail: heinrich@erdw.ethz.ch

C. A. Heinrich
Faculty of Mathematics and Natural Sciences,
University of Zürich, Zürich, Switzerland

Introduction

High-temperature porphyry Cu–Mo–Au deposits and lower-temperature high-sulphidation epithermal Cu–As–Au–Ag deposits are globally related, in space and time, to calc-alkaline hydrous magmas reaching the upper crust at convergent plate margins (Gustafson and Hunt 1975; Sawkins 1990; Hedenquist and Lowenstern 1994; Sillitoe 1997; Tosdal and Richards 2001; Sillitoe and Hedenquist 2003). The two deposit types are geologically distinct, but partly share the characteristic element association of Cu, Au and abundant sulphur, present in the form of sulphides and sulphates. The formation of Cu–Au deposits of both types is restricted to certain magmatic centres in certain segments of magmatic arcs. Both deposit types seem to form in crustal tectonic settings characterised by compression or near-neutral to locally extensional stress states, in contrast to regional extension which is typical for low-sulphidation deposits involving major meteoric fluid circulation (Tosdal and Richards 2001; Sillitoe and Hedenquist 2003). A confined stress environment, often associated with tectonic inversion, plate reorganisation or subduction flips, favours the development of sizable upper-crustal magma chambers as an essential source of saline hydrous fluids (Solomon 1990; Camus and Dilles 2001; Rohrlach 2003; Fournier 1999; Tosdal and Richards 2001, Fig. 1a). In individual ore districts, high-sulphidation epithermal and porphyry-type deposits can occur in intimate spatial association, but epithermal ore formation invariably overprints porphyry mineralisation at a given erosion level (Sillitoe 1994). The two deposit types may be almost coeval within the resolution of precise radiogenic age dating (e.g. <0.3 Ma age difference at Far South East—Lepanto: Arribas et al. 1995b; La Famatina: Losada-Calderòn and McPhail 1996), or epithermal ore formation may postdate exposed magmatism and porphyry ore formation by more than 1 m.y., i.e. significantly more than the maximum lifetime of a single upper-crustal magma chamber (e.g., Bendezu et al. 2003; Rohrlach 2003). Hot magmatic fluids, either single-phase (e.g., Rusk et al. 2004) or a high-salinity liquid coexisting with a lower-salinity vapour phase (e.g. Roedder 1971; Eastoe 1978; Ulrich et al. 2001; Redmond et al. 2004), are the dominant metal-precipitating agents in porphyry-style deposits, although a significant or even dominant proportion of the copper may be precipitated from lower-salinity aqueous fluids below 400°C (Reynolds and Beane 1985). Even cooler (<350°C) aqueous liquids forming high-sulphidation epithermal deposits predominantly have low to intermediate salinity, but stable isotope data show that these fluids also contain a significant or even exclusively magmatic water component (Giggenbach 1992; Rye 1993; Vennemann et al. 1993; Hedenquist et al. 1998; Kouzmanov et al. 2003). Quartz–sericite–pyrite $\pm$ chalcopyrite $\pm$ anhydrite veins cutting through potassic alteration in the upper parts of many porphyry deposits (Gustafson and Hunt 1975) are formed by fluids of similar salinity and isotopic composition (Hedenquist et al. 1998; Watanabe and Hedenquist 2001) and indicate an affiliation with the magmatic fluid component in high-sulphidation epithermal deposits (Sillitoe and Hedenquist 2003).

This paper explores the physical and chemical evolution of low-salinity to medium-salinity magmatic fluids along a range of possible ascent paths from their magmatic source at high pressures and temperatures to the near-surface domain, with the aim of clarifying the processes that may link epithermal gold deposits with the commonly associated porphyry-style deposits (Fig. 1). This modelling study is partly motivated by micro-analyses of fluid inclusions showing that high-temperature vapour-like fluids of low to intermediate salinity can carry extremely high concentrations of Cu, As and Au (Ulrich et al. 1999; Heinrich et al. 1999; Kehayov et al. 2003). Gold concentrations at ppm levels observed in natural fluid inclusions are consistent with experimental gold solubilities at near-magmatic temperatures (Loucks and Mavrogenes 1999), but far higher than those considered in earlier thermodynamic studies based on fluids in active geothermal systems (e.g. Krupp and Seward 1987; Spycher and Reed 1989) or considerations based on surface observations from volcanic fumaroles (e.g. Hedenquist et al. 1993, 1994a). Can gold and other essential ore components be transported to the low-temperature epithermal environment in high concentrations, as observed in some natural high-temperature fluids, without gradual dispersion along the flow path? Building on the study by Gammons and Williams-Jones (1997), a thermodynamic re-evaluation of this question is now possible, by combination of the new microanalytical inclusion data with a re-interpretation of fluid phase relations and recently published experimental data defining the thermodynamic stability of all relevant gold complexes across the decisive temperature range between 450°C and 200°C (Stefánsson 2003; Stefánsson and Seward 2003, 2004).

Published observations and interpretations

Kaolinite–alunite-type or high-sulphidation epithermal deposits were characterised and contrasted with the adularia-sericite or low-sulphidation type by Heald et al. (1987), White and Hedenquist (1990), Arribas (1995), Hedenquist and Richards (1998), Einaudi et al. (2003), Sillitoe and Hedenquist (2003) and others reviewing the terminology and increasing observational data about these endmember types of economically important precious-metal deposit. With increasing geological control on sampling, the interpretation of stable H and O isotope data from epithermal ore deposits has shifted from an emphasis on the role of meteoric water (e.g. Taylor 1974) to the recognition that magmatic fluids play a key role as metal contributors to epithermal

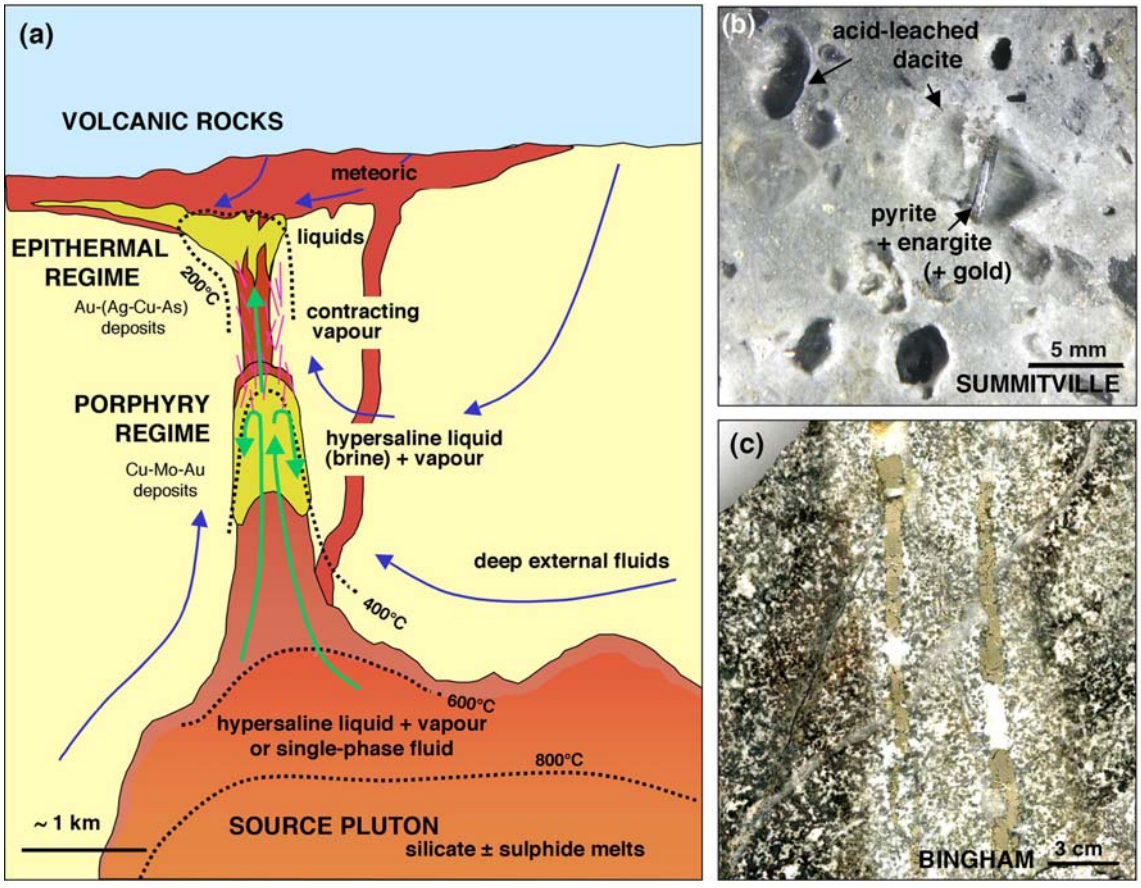

Fig. 1 Schematic cross section of a magmatic–hydrothermal system (**a**), and rock photographs showing typical vein and alteration relationships in porphyry-type and epithermal ore deposits (**b, c**). Three geological domains in Cu–Au mineralising magmatic–hydrothermal systems (**a**) include a large magma reservoir at depth, porphyry-style deposits located in cupolas and subvolcanic necks or dykes, and epithermal deposits located within 1–2 km of the land surface. In such systems, up to four types of hydrothermal fluid can interact with each other, depending on the pressure–temperature–depth distribution along the flow paths: single-phase magmatic fluid, hypersaline liquid or brine, vapour of variable density, and aqueous lower-salinity liquids that may be derived either from magmatic fluids (single-phase or vapour) or from groundwater penetrating downward from the hydrosphere (modified from Heinrich et al. 1999). **b** Typical paragenetic sequence observed in high-sulphidation epithermal deposits: late precipitation of enargite + pyrite (+ gold, not visible) into vuggy quartz, which resulted from earlier acid leaching (open cavities from dissolved former feldspars) and advanced argillic alteration of adjacent host rocks to quartz + kaolinite/dickite ± pyrophyllite ± alunite (Summitville, Colorado; see Stoffregen 1987). **c** Feldspar-destructive (sericite–quartz–pyrite) alteration along two vertical veins filled with quartz + pyrite + minor chalcopyrite and bornite, cutting earlier quartz stockwork veinlets associated with pervasive potassic alteration and disseminated chalcopyrite + bornite mineralisation (Bingham; see Redmond et al. 2004). Similar quartz–pyrite–sericite veins variably contribute to Cu ± Au ore grade in porphyry-style deposits (e.g. the Far South East porphyry associated with the Lepanto epithermal deposit, Hedenquist et al. 1998; or El Salvador: Gustafson and Hunt 1975). The early quartz veinlets contain coexisting vapour and hypersaline liquid inclusions, the later veins contain aqueous fluid inclusions of low to medium salinity. O–H-isotopes from similar veins elsewhere indicate dominantly magmatic water for all fluid types (e.g. Watanabe and Hedenquist 2001)

deposits, notably of the high-sulphidation type (Giggenbach 1992; Vennemann et al. 1993; Rye 1993; Kouzmanov et al. 2003). Current debate centres on the character and origin of this magmatic fluid component, and on the processes linking the igneous fluid source with the epithermal environment. Extending the "volatile transport" and "saline liquid transport" hypotheses reviewed by Arribas (1995) in the light of more recent data (e.g. Hedenquist et al. 1998; Heinrich et al. 1999; Muntean and Einaudi 2001; Kouzmanov et al. 2003), four endmember processes have been proposed for the sourcing and transport of gold and associated components into high-sulphidation gold deposits (Table 1). These endmember processes give different emphasis to the roles of rock leaching by meteoric fluids (1), entrainment of hypersaline magmatic liquid into surface-derived water (2), direct transfer of deeply-sourced single-phase igneous fluids (3), or a vapour phase ascending from a subjacent two-phase fluid environment (4). From the literature review summarised in Table 1, the following observations are particularly relevant in any attempt to identify the essential fluid processes leading to the formation of economic high-sulphidation gold deposits.D:\A + + Corrections\126\461

Field relations and paragenetic sequence of alteration and ore mineral deposition commonly record an early process of acid leaching of magmatic wall rocks to form vuggy quartz ± alunite along pathways of strong fluid

Table 1 Review of observations and interpreted fluid processes contributing to the formation of high-sulphidation epithermal gold deposits

Proposed process	Evidence	Deposit, district	Important publications
Advanced argillic/acid sulphate alteration and leaching to "vuggy silica"			
Low-density magmatic vapour ascends and mixes with variable fractions of near-surface meteoric water	Geological field relations	Goldfield NV	Ransome (1907)
	$NaCl–H_2O$ fluid stability relationships		Henley and McNabb (1978)
	Mineral and fluid thermodynamics	Butte, Montana Summitville Colorado	Brimhall and Ghiorso (1983) Stoffregen (1987);
	O–H isotopes	Pueblo Viejo, Dominican Republic	Rye (1993); Vennemann et al. (1993)
	Active volcanoes	White Island, New Zealand	Giggenbach (1992); Hedenquist et al. (1993)
		Kawah Ijen, Indonesia	Delmelle and Bernard (1994)
		Satsuma Iwojima, Japan	Hedenquist et al. (1994a)
Cu–As–Au sulphide introduction and ore deposition			
Metal introduction, gold and sulphide precipitation occurs slightly after advanced argillic alteration, by:	Cross-cutting relations and textural observation	Summitville, Colorado Chinkuashih, Taiwan Furtei, Sardinia, Italy and many other sites	Stoffregen (1987) Wang et al. (1999) Ruggieri et al. (1997) Arribas (1995) for review
(a) Flooding of magmatic–hydrothermal system with *rock-interacted meteoric water*, after acquisition of ore metals by leaching.Gold precipitation by boiling, fluid mixing, or acidification through reaction with argillic wall rocks, or by mixing with acid near-surface waters	Mineral stabilities: presence of sericite ± feldspar alteration assemblages below the near-surface advanced argillic and high-sulphidation ore zones	Summitville	Stoffregen (1987) Berger and Henley (1989); See also Arribas et al. (1995a): Rodalquilar
	O–H isotopes: variably rock-exchanged meteoric water involved in ore deposition	Goldfield, Nevada	Taylor (1974)
	Ore-stage silicate assemblages indicating less acid and less oxidised fluid compared with preceding advanced argillic alteration		Stoffregen (1987, Fig. 13) Berger and Henley (1989)
	Thermodynamic modelling based on active geothermal fluids		Spycher and Reed (1989)
(b) Ascent of *hypersaline magmatic liquid (brine)* and its entrainment into meteoric fluids	Hypersaline liquid inclusions (halite and sulphur daughter crystals) with low-salinity vapour-rich and aqueous inclusions, in quartz immediately postdating pyrite-enargite-gold, trapped at ~275°C	Nansatsu district, Japan	Hedenquist et al. (1994b)
	Hypersaline liquid inclusions occurring predominantly in sericite alteration below high-sulphidation epithermal deposit, trapped in state of mixing with low-salinity to medium-salinity aqueous fluids	Rodalquilar Buffalo deposit, Chinkuashih, Taiwan	Sänger von Oepen et al. (1989) Arribas et al. (1995a, Fig. 16) Wang et al. (1999, Fig. 2f)
(c) Introduction of a *single-phase magmatic fluid of intermediate-salinity*.Bulk fluid extraction from residual melt, as magma crystallisation front retracts to depth, allowing unseparated fluid exsolution from the melt	Thermal modelling, consistent with isotopically magmatic 5% salinity fluid and vein overprinting observations	Lepanto—FSE system, Philippines	Hedenquist et al. (1998); Shinohara and Hedenquist (1997)
	Alteration and-vein timing relationships	Maricunga Belt, Chile	Muntean and Einaudi (2001)
	Melt-fluid partitioning experiments indicating low-salinity fluids can separate late during magma crystallisation at pressures > 1 kbar	Experiments and numeric modelling	Kilinc in Burnham (1979) Cline and Bodnar (1991)
(d) Cu–As–Au and S introduction in a low-salinity to intermediate-salinity fluid originating by *separation of a magmatic vapour phase from a denser hypersaline liquid*, at high temperatures and pressures similar to those associated with potassic alteration in porphyry-type deposits	Geology: massive sulphide pyrite-enargite-gold bodies with subordinate quartz above porphyry-type Cu–(Au) deposits	Lepanto, Philippines Frieda River, Papua New Guinea Bor, Serbia; Recs, Hungary	Sillitoe (1983) quoting Henley and McNabb (1978) and Eastoe (1982) for discussion of metal transport by high-density vapour

Table 1 (Contd.)

Proposed process	Evidence	Deposit, district	Important publications
	Geologic environment reminiscent of the top of a porphyry system ('vapour', without specifying separation from a more saline liquid)	Tampakan, Philippines	Rohrlach (2003)
		Ore stages at Pueblo Viejo, Dominican Republic	Muntean et al. (1990)
		Mole Granite, Australia	Audétat et al. (2000, 1998)
	Preferential partitioning of Cu ± As ± Au into intermediate-salinity vapour phase of coexisting hypersaline liquid + vapour inclusion assemblages: Au in vapour to 10 ppm; liquid enriched in Na, K, Fe, Mn, Pb, Zn	Alumbrera, Argentina; Grasberg, Irian Jaya	Ulrich et al. (2001)
			Ulrich et al. (1999)
		Several other Sn–W and Cu–(Mo–Au) deposits	Heinrich et al. (1992, 1999)
	Significant metal volatility in experiments with high water fugacity	Experiments	Williams-Jones et al. (2002)
	Dominant low-salinity to medium-salinity aqueous inclusions and rare coeval hypersaline liquid inclusions on mixing trends: two fluids of different salinity coexist in fluid source below epithermal deposits	Rodalquilar	This study, Fig. 2, and discussion in the text
		Chelopech	
		Tampakan	
		Chinkuashih possibly Nansatsu	

focussing (Fig. 1b), usually surrounded by haloes of advanced argillic alteration (quartz + kaolinite/dickite/pyrophyllite + alunite). There is general agreement that this alteration is caused by low-density HCl–SO_2–H_2S-rich magmatic vapour, condensing and commonly mixing with surface-derived groundwater (Brimhall and Ghiorso 1983; Stoffregen 1987; Hedenquist et al. 1993, 1994a; Delmelle and Bernard 1994; see Table 2 for fluid phase and process terminology used throughout this paper). Acid leaching is followed by later precipitation of sulphides, usually starting with ubiquitous but variably abundant pyrite and followed successively by enargite, base metals including tennantite, and most of the gold that is present in economic deposits (Stoffregen 1987; Muntean et al. 1990; Claveria 2001). Uneconomic vuggy quartz ± pyrite is far more common than orebodies containing additional Cu–As-sulphides and economic gold concentrations. The local predominance of muscovite-illite in orebodies with the highest-grade gold orebodies (e.g. El Indio: Jannas et al. 1990; Pepa in the Maricunga district: Muntean and Einaudi 2001, p. 755), and zones of muscovite-stable alteration underlying some epithermal ore deposits hosted within zones of advanced argillic alteration (Arribas et al. 1995a) are consistent with chemical evolution toward less acidic, and commonly also more reduced and sulphur-depleted fluids during the economic ore deposition stage (Stoffregen 1987; Claveria 2001; Einaudi et al. 2003).

Fluid inclusion and stable isotope data from high-sulphidation gold deposits are mainly recorded by quartz crystals postdating the crypto-crystalline residual quartz resulting from acid leaching, and by infrared-transparent sulphide crystals (enargite, pyrite) related to or slightly postdating the economic ore introduction stage. In Fig. 2, published microthermometric datasets from seven well-studied ore districts have been compiled on the same scale, illustrating significant communalities in temperature–salinity relationships despite local differences. Common to all deposits is an array of fluids along a more or less well-defined correlation trend (heavy double arrow, Fig. 2f) between essentially pure water (M), which in some cases is isotopically identified without ambiguity as meteoric water, and a higher-temperature liquid of low to medium salinity (2–10 wt%; L) with an isotopically magmatic signature. Correlations with spatial zonations (Mancano and Campbell 1995) and O–H isotope data (Rohrlach 2003; Kouzmanov et al. 2003) indicate that this trend is due to dilution of a hot magmatic fluid of relatively low salinity (L) by cooler meteoric groundwater (M) at the site of ore deposition. In some deposits, a slightly more saline fluid is associated with a texturally earlier enargite stage, followed by lower-salinity fluid of similar temperatures during high-grade gold deposition (e.g. 3–4% decreasing to 1.4% NaCl eq. in distinct vein sets at El Indio; Jannas et al. 1990). Many but not all high-sulphidation epithermal deposits contain a subordinate number of much higher-salinity liquid inclusions. In some deposits such hypersaline inclusions are confined to texturally distinct

Table 2 Terminology of fluid phases and interaction processes in saline hydrothermal systems

Fluid phase definitions	
Fluid	Any mobile phase dominated by volatile constituents of the H–O–C–N–S system (e.g., H_2O, CO_2, N_2, H_2S, SO_2...) with variable concentrations of dissolved components such as chloride salts, etc.
Single-phase fluid	A fluid of any composition at a pressure above (or a temperature below) the two-phase (liquid + vapour) surface
Liquid	A water and salt-rich fluid with a density above the critical density of the corresponding salt–water mixture (e.g. $\rho_{crit} = 0.32$ g cm^{-1}for pure water; $\rho_{crit} = 0.48$ g cm^{-1}for 7 wt% NaCl; $\rho_{crit} = 0.59$ g cm^{-1}for 20 wt% NaCl)
Hypersaline	Specifies a liquid with > 26% NaCl (commonly called "brine"; halite saturated at room temperature)
Aqueous	Specifies a dense water-rich (< 26% NaCl) liquid at temperatures well below the critical point of water (374°C/225 bar) and pressures at or above the boiling curve of water
Vapour	A water and variably salt-rich fluid (± CO_2 and other gases) with a density below the critical density of the corresponding salt–water mixture
"Supercritical fluid" is avoided in this paper because it cannot be defined with reference to P and T for binary or multicomponent fluid systems. For pure water, supercritical refers to a fluid at pressures and temperatures above the critical point of the substance	
Fluid interaction processes	
Mixing	Homogenisation of two compositionally different fluid phases to a single phase (e.g. mixing of magmatic vapour with aqueous liquid of meteoric origin below a geothermal hot spring)
Phase separation	Separation of an initially homogeneous fluid into two or more phases, without further specification of the physical process
Condensation	Specifies a phase separation process in which an initially homogeneous fluid nucleates droplets of aqueous liquid or brine (e.g. phase separation by intersection of the NaCl–H_2O two-phase surface on the low-salinity or "dew-point" side of the critical curve)
Boiling	Specifies a phase separation process of an initially homogeneous fluid into two phases by formation of bubbles of vapour or steam (e.g. phase separation by intersection of the NaCl-H_2O two-phase surface on the high-salinity or "bubble-point" side of the critical curve)
Contraction (<–> expansion)	Density increase (<–> decrease) without intersection of any phase boundaries (e.g. contraction of a single magmatic volatile phase or a vapour to an aqueous liquid, by cooling along any pressure path above the two-phase curve of the H_2O–salt (–gas) system)

The following definitions do not uniquely subdivide the pressure–temperature–composition (*P–T–X*) space of possible fluid properties in natural hydrothermal systems, but this ambiguity is an inherent feature of salt–water phase relations at high temperatures and pressures (Fig. 3)

samples that may have been mechanically transported to the site of the epithermal orebody (Ruggieri et al. 1997, Fig. 2b), or are restricted to texturally earlier and spatially separate veins related to porphyry-style potassic alteration (Hedenquist et al. 1998; Rohrlach 2003, Fig. 2d). Figure 2 shows that many high-sulphidation epithermal deposits, and even single samples, also display distinct but locally variable mixing lines along the steep grey arrows in Fig. 5f, between the hypersaline inclusion array and the lower-salinity array trending along the black double-pointed arrow (Sänger von Oepen et al. 1989; Arribas et al. 1995a, Fig. 2a; Moritz et al. 2003, Fig. 2c; Wang et al. 1999, Fig. 2e; see also Hedenquist et al. 1994b for the Nansatsu district, Japan, and P. Bethke and R. Rye (personal communication) for Summitville). Such steep mixing trends, if confirmed for assemblages of coeval inclusions, would indicate that hypersaline liquid was intermittently introduced together with the low-salinity to medium-salinity fluid L. If both L and B are magmatic fluids introduced together, they must have coexisted as immiscible phases at depth and become miscible again in the epithermal domain, which is very plausible in the light of the fluid-phase relations discussed below. Alternatively, they may originate from entirely separate but simultaneously active magmatic sources at depth. Some exceptionally high-grade epithermal gold deposits of low to intermediate sulphidation character also contain evidence for intermittent incursion of potentially magmatic fluids with a similar restricted salinity ranges (e.g. Porgera: 3–5 and 6–9 wt% NaCl eq., Richards et al. 1997; Ronacher et al. 2004; Sacarimb: mostly 2–6 wt%, Alderton and Fallick 2000), and the same salinity range is seen in Carlin-type gold deposits, although these generally have no obvious association with a proximal magmatic fluid source (Cline and Hofstra 2000: 3–9 wt% NaCl eq.).

*Active volcanic systems*confirm that acid alteration (Delmelle and Bernard 1994) and high-sulphidation ore formation must be considered as two distinct processes. Hedenquist et al. (1994a) showed that the Satsuma Iwojima volcano generated a significant mass of residual silica by quiescent degassing and acid leaching, but neither the low-density vapour nor the acid-enriched meteoric water would be capable of forming an economic orebody in the likely lifetime of the magmatic–hydrothermal system. Denser and more saline fluids

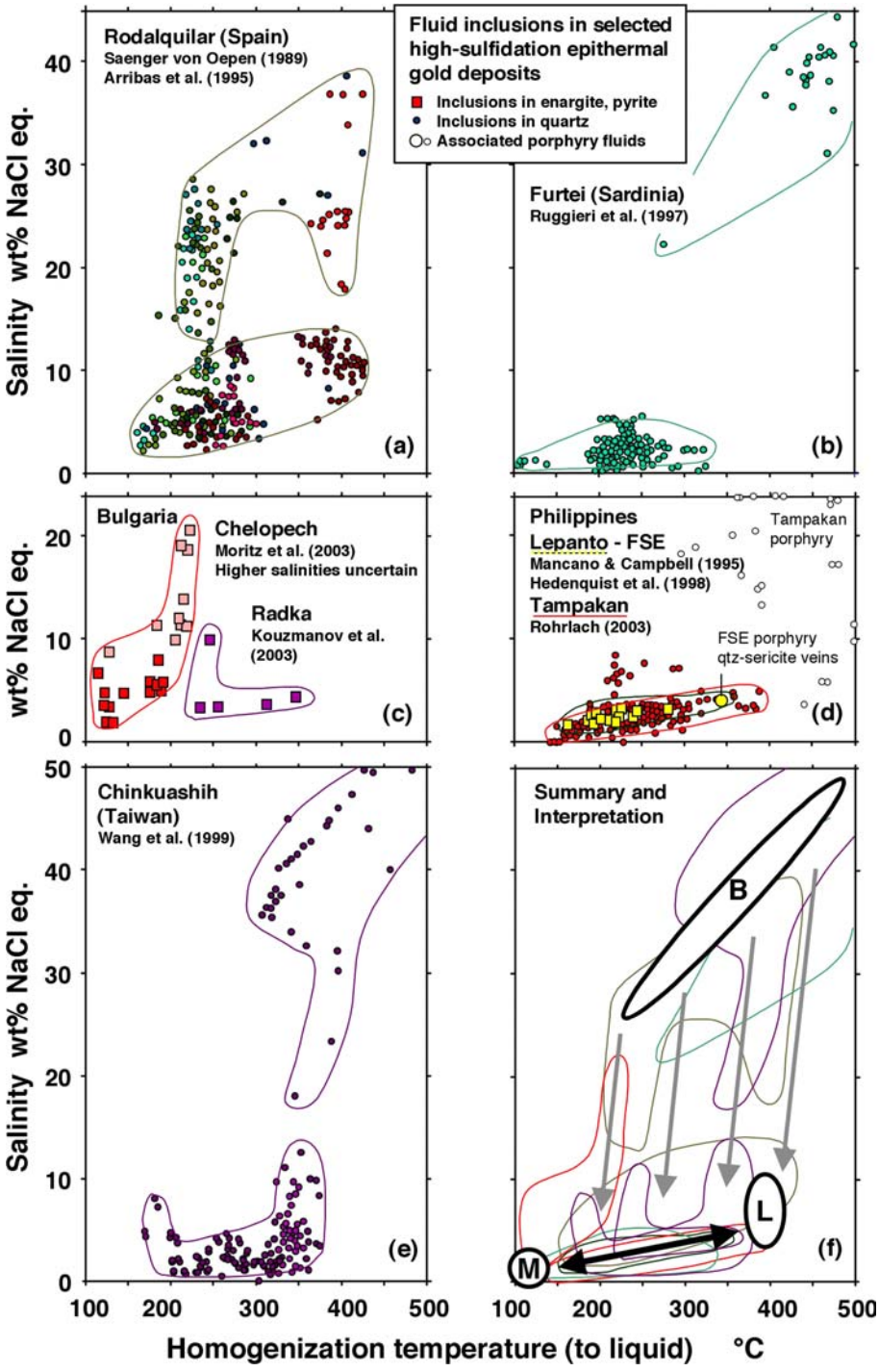

Fig. 2 Compilation of published fluid inclusion data for high-sulphidation gold deposits. Apparent salinities versus homogenisation temperatures of liquid-rich inclusions (**a**–**e**), and a summary diagram of all data together with a proposed interpretation of the main fluid endmembers and interaction processes (**f**) are plotted on the same scale. Most epithermal deposits record an interpreted mixing trend between a hot low-salinity to intermediate-salinity magmatic fluid "*L*" and cooler essentially salt-free meteoric water "*M*" (*black double-arrow* in **f**). Inclusions above 15% salinity are subordinate but widespread, and locally exhibit steep linear trends between hypersaline liquid (brine, "*B*") and the lower-salinity array "*L*–*M*". This may indicate re-mixing at epithermal *P*–*T* conditions of liquids that had coexisted as immiscible vapour and hypersaline brine at higher temperature in the deeper part of the magmatic–hydrothermal system

have much greater capacity to transport significant amounts of metals (Hemley et al. 1992; Williams-Jones et al. 2002), and this fact is reflected by the much greater quantity of ore metals ejected as aerosols during vigorous eruption (e.g. White Island: Hedenquist et al. 1993) compared with passive degassing by low-density vapour (e.g. Satsuma Iwojima: Hedenquist et al. 1994a).

This review of observations summarised in Table 1 and Fig. 2indicates that a variably hot, low-salinity to medium-salinity aqueous liquid (L) of magmatic origin is widespread in epithermal gold deposits, and that this is probably the essential metal-introducing agent at least for high-sulphidation gold deposits. Several or all of the proposed endmember processes summarised in Table 1, involving meteoric water and magmatic vapour, hypersaline liquid and single-phase fluids, are probably active to variable degrees in different parts of a magmatic–hydrothermal system or at different stages in its evolution, but not all may be equally essential for economic gold enrichment. The approach of the following

analysis is therefore not to exclude or ignore a particular process, but to investigate which is likely to be the *most effective in forming an economic epithermal gold–(arsenic–copper) deposit* within the constraints of physical, chemical and geological observation.

Fluid-phase evolution: terminology and processes

Before discussing metal solubility and chemical reactions between fluids and rocks at the magmatic to epithermal transition, the fluid stability relationships and the possible physical evolution paths of magmatic–hydrothermal fluids must be clarified (Table 2). Magmatic volatiles separating from calc-alkaline magmas predominantly consist of water and chloride salts, and magmatic fluids are therefore commonly discussed with reference to the experimentally well-studied phase relations in the binary system NaCl–H_2O (Bodnar et al. 1985; Fournier 1987; Anderko and Pitzer 1993b; Driesner 2001; Driesner and Heinrich 2002, Fig. 3). Expression of fluid salinities as NaCl *equivalent* wt% is useful for interpretation of fluid evolution from inclusion microthermometry (Bodnar and Vityk 1994), even though quantitative pressure–temperature–composition (*P–T–X*) relationships are significantly shifted by the fact that NaCl commonly constitutes less than half (by weight) of the salts present in natural magmatic fluids, and by the common presence of other volatiles including CO_2 and sulphur species.

Phase stability relations in the NaCl–H_2O model system

A key feature of fluid-stability relationships in the NaCl–H_2O system is a large region of partial miscibility of two phases extending to pressures far higher than the triple points of the two endmembers (Bodnar et al. 1985). The *critical curve* is defined as the locus of points of maximum pressure (or minimum temperature) at which a fluid of given salinity can separate into two phases. This is shown by the red crest line of the two-phase surface (black grid in Fig. 3), swinging across the phase diagram from pure water toward higher NaCl contents. At any *P–T–X* point below the two-phase surface, two fluids will coexist, a *vapour* phase of lower density and NaCl salinity, and a *liquid* phase of higher density and salinity. The terms vapour and liquid can also be applied more generally to single-phase fluids that exist at pressures above the two-phase surface: vapour-like fluids having a density lower than the critical density of the corresponding composition, liquid-like fluids having a density greater than the corresponding critical density (see Table 2a for examples). In fluid-inclusion petrography, "brine" is used interchangeably with the more clearly defined term *hypersaline liquid*, specifying a salinity that exceeds the solubility of halite at room temperature (26% NaCl; Bodnar and Vityk 1994).

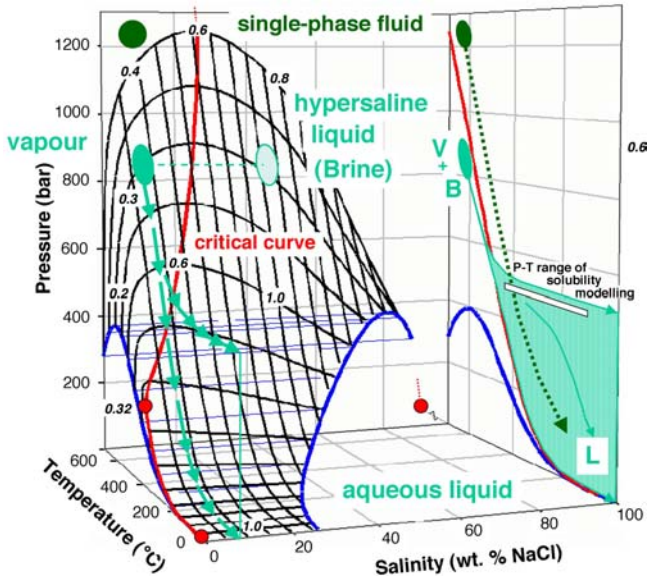

Fig. 3 Phase stabilities in the NaCl–H_2O model system shown in pressure–temperature–salinity space, with a perspective representation of the two-phase immiscibility surface (coexisting vapour + -liquid; *gridded by black isopleths and isotherms*) and the limiting surface of halite saturation at low pressures (blue; Driesner 2001; Driesner and Heinrich 2002). The critical curve (*heavy red line at the crest of the two-phase surface*) swings from high salinities at high pressures and temperatures (~25 wt% NaCl at the limiting back surface of the diagram) across to low salinities at low pressures and temperatures. Approximate fluid densities (g cm^{-3}) along the two-phase surface are indicated by *small numbers in italics*. Any high-temperature vapour-like fluid of low to medium salinity, originating from slightly above or coexisting with hypersaline liquid along the two phase surface, can be cooled and contracted to an aqueous liquid without heterogeneous phase changes, if the pressure above the two-phase surface remains below ~450°C, as indicated by *strings of green arrows* for two limiting *P–T* paths and by the *green area* in the *P–T*projection on to the right side of diagram. For typical depths of the porphyry to epithermal transition (1–3 km), this *vapour contraction* (Heinrich et al. 2004) requires that the low-salinity to intermediate-salinity fluid cools at least initially at near-lithostatic fluid pressure, along *P–T* paths that are very similar to the paths required for direct transfer of a single-phase magmatic fluid to aqueous liquid (*stippled green arrowS–L*; Hedenquist et al. 1998)

The term "supercritical fluid" cannot be unambiguously defined in the binary NaCl–H_2O system and should best be avoided in discussions of magmatic–hydrothermal systems, because the single-phase region is completely continuous between fluids of low and high salinity, and between fluids of vapour-like and liquid-like density. This fact is particularly relevant in the discussion of moderately saline fluids, which can exist as a vapour phase at or slightly above the two phase curve at high pressure and temperature, or alternatively—but without any intervening phase boundaries!—as an aqueous liquid at low temperatures. The more general term *single-phase fluid* is used here for any fluid existing well above the two-phase surface, unless vapour-like or liquid-like density is emphasised. This includes (but is not restricted to) inclusion fluids that homogenise by

meniscus fading on heating, because their isochores intersect the two-phase surface in the vicinity of the critical curve.

Mixing, boiling, condensation, and vapour contraction

Cl/OH ratios in amphiboles suggest that the average chloride:water ratio in calc-alkaline magmas is slightly greater than in seawater (Burnham 1997, p. 112). The bulk salinity of the magmatic fluids is therefore believed to be typically between 5 wt% and 10 wt% NaCl equivalent (Burnham 1979; Cline and Bodnar 1991; Hedenquist and Lowenstern 1994), although deviations from this range do occur and may well be significant for ore formation (Audétat and Pettke 2003; Cline and Bodnar 1994; Ulrich et al. 2001). Fluid inclusion observations from the deeper parts of some porphyry copper deposits show that the ascending magmatic fluid may initially be a single-phase fluid of intermediate density and less than 12 wt% equivalent salinity (e.g. Bingham, Utah: Redmond et al. 2004; Butte, Montana: Rusk et al. 2004). In other porphyry deposits the earliest-recorded fluid is a hypersaline liquid (e.g. Bajo de la Alumbrera: Ulrich et al. 2001), and some deposits show melt inclusion evidence that coexisting hypersaline liquid and vapour separated directly from silicate melt (e.g. Audétat and Pettke 2003), consistent with experimental evidence that the solidus of granodioritic magmas intersects the two-phase surface of the salt–water system at pressures near 1 kbar (Bodnar et al. 1985).

Depending on rather small differences in the exact pressure–temperature path experienced by fluids ascending from their igneous source to the Earth's surface, significantly different phase evolutions can occur. A single-phase fluid can evolve to an aqueous liquid, if it cools at sufficient pressure never to intersect the two-phase surface (e.g. Hedenquist et al. 1998). If a single-phase fluid of high initial salinity breaches the two-phase surface on the liquid side of the critical curve, some lower-salinity vapour phase will separate out by a process that involves nucleation of bubbles, and is therefore called *boiling* (e.g. Alumbrera: Ulrich et al. 2001). Alternatively, if a single-phase igneous fluid with low to intermediate salinity (up to ~20 wt% NaCl at high P) breaches the two-phase surface at any point on the vapour side of the critical curve it will separate into a somewhat less saline vapour by *condensation* of droplets of liquid with higher salinity (e.g. Panguna: Eastoe 1978, 1982; Bingham: Redmond et al. 2004). Depending on hydrologic conditions (temperature–pressure–permeability relationships), any vapour existing at some point on the lower-salinity side of the critical curve can depart from the two-phase surface, become physically separated from the liquid, and cool in the single-phase field en route to the surface. It will thereby evolve from a low-density vapour to an aqueous liquid without any change in salinity, by passing above the critical curve. This process is termed *vapour contraction* (Heinrich et al. 2004), to emphasise the important difference from the phase separation process of condensation (Table 2).

For illustration in Fig. 3 and for all subsequent multicomponent modelling, a medium-salinity fluid with 7 wt% NaCl (equivalent) is considered, which is similar to single-phase fluids recorded in the porphyry-Cu–Mo stage of Butte (Rusk et al. 2004) and vapour inclusions trapped together with hypersaline liquid inclusions in pre-sulphide vein quartz at Grasberg (Ulrich et al. 1999, Table 3). At potential magmatic source conditions for Butte of 800°C and pressures of ~2,000 bar, such a fluid has a density of 0.48 g cm^{-3} (Anderko and Pitzer 1993a, b; Driesner 2001). At 650° and 930 bar, a similar fluid has a density of 0.34 and can coexist with a liquid having a salinity of ~40 wt% NaCl. If the vapour phase physically separates from the saline liquid and subsequently cools in the single-phase field, it will gradually contract to a density, for example, of 0.57 g cm^{-3} at 450°C and 500 bar where it would cross about 70 bar above the critical curve. Upon further isobaric cooling it will reach typical liquid-like densities (e.g. 0.85 at 300°C; 0.97 at 200°C; Anderko and Pitzer 1993a, b; Fournier 1999; Driesner 2001). Pressure, during cooling anywhere within the green hachured *P–T* area of Fig. 3, becomes progressively less influential due to the decreasing compressibility of aqueous liquids with falling temperature. As soon as the vapour has contracted to a liquid by crossing above the critical curve, it can *mix*, in any proportion, with other liquids including variably heated meteoric groundwater. This is consistent with fluid inclusion evidence indicated by the black double-arrow M–L in Fig. 2f. It also becomes completely miscible again with any previously separated hypersaline liquid, which may be indicated by the steep grey mixing trends in Fig. 2f. At low pressures and epithermal temperatures, the vapour-derived low-salinity to medium-salinity fluid may also *boil* again, by separation of essentially salt-free vapour from the aqueous liquid.

The possibility of a low-salinity to medium-salinity fluid crossing from the vapour side (coexisting with a hypersaline liquid) to the aqueous liquid side (potentially boiling off low-density vapour), is a consequence of the strong compositional dependence of the critical curve in *P–T–X* space (Fig. 3). Note that *P–T* paths generating a low-salinity to medium-salinity aqueous liquid departing from the vapour side of the two-phase surface (Sillitoe 1983; Heinrich et al. 1999, 2004) are very similar to *P–T* paths generating an epithermal liquid from a single-phase magmatic fluid (Hedenquist et al. 1998; Muntean and Einaudi 2001). While the two physical processes proposed by these authors for the origin of epithermal ore fluids are quite similar (and therefore require similar geological conditions), the chemical consequences with regard to minor volatiles and ore metal components may be decisively different, as shown by the following thermodynamic reaction calculations.

High-temperature magmatic fluid compositions

High-temperature laboratory experiments (Burnham 1979; Candela and Piccoli 1995) and fluid-inclusion studies (Roedder 1971; Wilson et al. 1980; Rankin et al. 1992; Heinrich et al. 1999) show that the major salt components in magmatic fluids are NaCl, KCl and $FeCl_2$ in comparable concentrations (up to tens of weight percent in hypersaline magmatic liquids), followed by $MnCl_2$, $CaCl_2$ and ore metals commonly reaching concentrations of thousands of ppm to a few weight percent. Volatiles, notably CO_2 and sulphur species, also may constitute several weight percent, as indicated by CO_2 clathrates in porphyry-related and epithermal fluid inclusions (Redmond et al. 2004; Ronacher et al. 2004) and by abundant sulphur in fumarolic emanations. Magmatic fluid composition may vary with progressive crystallisation of the magma, distillation models predicting selective enrichment of chloride and volatile components in early fluid batches and progressively more water-rich compositions during the later stages, at least during single-phase fluid exsolution at $P > 1$ kbar (Cline and Bodnar 1991). However, exsolving fluids may not be expelled and focussed into mineralised structures as physically separate batches, once the magma chamber changes from convection to wholesale crystallisation (Shinohara and Hedenquist 1997). To a first order, therefore, average compositions of magmatic–hydrothermal fluids are estimated from experimental, volcanic gas and fluid inclusion data, as a starting point for thermodynamic modelling of their chemical evolution during cooling and wall rock interaction on the way to the epithermal environment.

Compositional constraints from experiments and active volcanic systems

Experimental equilibration studies among silicate melts, hydrous fluids and minerals at magmatic temperatures define the major-element concentrations including Na/K/Ca ratios (Burnham and Ohmoto 1980; Burnham 1997), HCl/KCl and HCl/NaCl ratios (Williams et al. 1997; Frank et al. 2003) and some ore metal contents in magmatic fluids (Candela and Piccoli 1995; Williams et al. 1997; Frank et al. 2002, Table 3).

Because of the early saturation of typical calc-alkaline melts in magnetite, the iron concentration of magmatic fluids is controlled by magnetite solubility equilibria rather than by melt-fluid partitioning (Candela 1989: $Fe_3O_4 + 3HCl = 3FeCl_2 + 1.25O_2 + 1.5H_2O$). The iron concentration in fluids coexisting with granodiorite magma near the upper f_{O2} stability limit of magnetite is sensitive to total chloride content of the fluid (Chou and Eugster 1977). About 0.2*m* Fe is expected in a magmatic fluid with 1.2*m* Cl (equivalent to ~7 wt% NaCl eq.; Burnham and Ohmoto 1980, Fig. 6; Burnham 1997, p. 115).

Controls on the concentration of the high-temperature sulphur species, SO_2 and H_2S, in the magmatic volatile phase of subduction-related igneous systems are not fully understood (Carroll and Webster 1994). The assemblage pyrite + magnetite + pyrrhotite would maximise SO_2 and H_2S fugacities and buffer their ratio by the reactions like $Fe_3O_4 + 5FeS_2 = 8FeS + 2SO_2$and $FeS_2 + 2FeS + 4H_2O = Fe_3O_4 + 4H_2S$ (Burnham and Ohmoto 1980). The activities of both sulphur species and the SO_2/H_2S ratio increase with temperature, to reach sub-equal concentrations in water-rich fluids at near-magmatic temperatures (Giggenbach 1980; Taran et al. 1995; Fournier 1999). Comparable concentrations of H_2S and SO_2 are indeed back-calculated from fumarolic gases emitted by calc-alkaline volcanoes (reviewed by Symonds et al. 1994, Table 3 and Fig. 14a). Experimentally measured (Ding and Seyfried 1992; Hemley et al. 1992) and calculated solubilities (e.g. using SUPCRT95) of pyrite + magnetite + pyrrhotite in chloride-bearing fluids rise to very high concentrations above 500°C, such that pyrite is initially far undersaturated. Saturation of magmatic pyrrotite or an iron sulphide melt does occur at certain stages in the evolution of calc-alkaline magmas, as indicated by inclusions in phenocrysts (Hattori and Keith 2001; Halter et al. 2002; Core et al. 2004). Anhydrite is observed as phenocryst and matrix phase in highly oxidised volcanics and subvolcanic intrusives (Carroll and Rutherford 1987; Hattori and Keith 2001; Audétat et al. 2002). Cryptic anhydrite saturation may be widespread as a transient phenomenon as indicated by high and variable sulphate concentrations in igneous apatite associated with the porphyry-copper mineralising magmas at Yerington (Streck and Dilles 1998), and the composition of magmatic sulphide melts in the Farallòn Negro Volcanic Complex seems to require an external source of sulphur in these porphyry-mineralising magmas (Halter et al. 2004). These observations indicate that H_2S and possibly also SO_2 concentrations in the magmatic volatile phase of calc-alkaline systems are primarily limited by sulphur availability in the melt, rather than by partitioning and mineral solubility equilibria. sulphur solubility experiments in trachyandesite melts from El Chichon at variable f_{O2} (Carroll and Rutherford 1987; Luhr 1990) may serve as an indication of maximum sulphide and sulphate availability at conditions of single-phase magmatic fluid saturation near 800°C. Solubilities of sulphate (at f_{O2}~HM) and sulphide (at NNO) are of similar magnitude, a few 100 ppm each (Carroll and Webster 1994, pp 242–243, Fig. 11). Assuming that 400 ppm H_2S and SO_2each are taken up by 5% water exsolving from the silicate melt, concentrations in the fluid of 0.4 wt% H_2S and 0.8 wt% SO_2, or 0.2 m each on a molal scale, would result. Experimental upper limits for sulphide and sulphate solubility in Fe-free haplogranite systems (Keppler 1999) are consistent with these estimates.

Iron and sulphur concentrations in upper-crustal magmatic fluids are subject to uncertainty and possibly

significant variation. Nevertheless, the first-order conclusion here is that $FeCl_2$, H_2S and SO_2, whose mass-balance critically determines the fate of magmatic–hydrothermal fluids as shown below, probably occur at comparable concentrations. A ratio of $Fe:S_{tot}\sim1$ would also result if both components in the fluid were predominantly derived by destabilisation of a magmatic sulphide phase (~FeS; Halter et al. 2002). Any processes affecting their early separation from each other are therefore of particular importance for hydrothermal ore formation.

Ore-metal concentrations from microanalysis of fluid inclusions

Elemental analysis of fluid inclusions has shown that magmatic–hydrothermal fluids can contain very high concentrations of base and precious metals, prior to reaching saturation with ore minerals. Mineral precipitation, where directly monitored by paragenetic sequence, involves drastic drops in metal concentration in the fluid, sometimes over several orders of magnitude (Audétat et al. 2000; Ulrich et al. 2001; Landtwing et al. 2004). This implies that mineralising magmatic fluids may be commonly far out of thermodynamic equilibrium with the final mineral assemblage at the ore deposition site.

Some of the highest copper and gold concentrations ever recorded in a natural hydrothermal fluid occur in vapour inclusions (density 0.2 ± 0.1 g cm^{-3} estimated from degree of filling at room temperature) in quartz crystals texturally predating high-grade chalcopyrite deposition in the Grasberg porphyry-Cu–Au deposit (Ulrich et al. 1999; Table 3). These inclusions occur together with high-salinity liquid inclusions (68–76 wt% NaCl eq., $T_h\sim650$°C) that contain higher concentrations of Na, K, Fe, Mn and other heavy metals. The presence of CO_2 clathrate in the vapour inclusions, the general difficulty of observing salt melting in inclusions with a small liquid fraction at low temperature, and the uncertainties of applying NaCl–H_2O phase relations to fluids in which NaCl constitutes only one third of the total solute content hamper quantitative interpretation of these inclusion relationships. The possibility cannot be ruled out that this low-density fluid records an initially one-phase fluid from which the hypersaline liquid was in the process of separating, which would be consistent with considerable variation in salinity and metal ratios found in recent studies of other samples from this deposit (Williams et al. 2003). As with all LA-ICPMS analyses of such complex low-density fluids, element ratios and the relative enrichment of Cu, As and Au in the low-density vapour, compared with enrichment of NaCl, KCl and $FeCl_2$ in the coexisting hypersaline liquid, are better defined than their absolute concentrations.

The densities, apparent salinities and microthermometric properties of the Grasberg inclusions are typical of early high-temperature liquid and vapour inclusions coexisting in other shallow porphyry-Cu deposits (Roedder 1971; Bodnar 1995), but the salinity of the Grasberg vapour is also in the range of single-phase magmatic fluids. In terms of their Na/K/Fe/Cu ratio, they are similar to concentrations estimated from experimental data and analyses of significantly denser (~0.4–0.65 g cm^{-3}) and somewhat lower-salinity (3–5% NaCl eq.) single-phase ore fluids in the deep-seated porphyry-Cu–Mo deposit at Butte (Rusk et al. 2004). LA-ICPMS analyses of iron concentrations in those inclusions are in agreement with the experimental data of Burnham and Ohmoto (1980, Fig. 6) for single-phase magmatic fluids at the corresponding salinity.

sulphur cannot be analysed by LA-ICPMS at useful detection limits. Large chalcopyrite daughter crystals indicate that Cu and reduced sulphur in some porphyry-hosted vapour inclusions is higher, in mass proportion, than in coexisting hypersaline liquid inclusions (Etminan 1977; Sawkins and Scherkenbach 1981). High but poorly quantified sulphur concentrations also occur in ore-stage fluids of some high-sulphidation epithermal deposits, as recorded by quadrupole mass spectrometry of gas extracts (Wang et al. 1999). sulphur species concentrations currently remain the least-constrained of all input properties of magmatic–hydrothermal Cu–Au systems, and thus become critical input assumptions to be explored by reaction modelling. With this aim, the chemical evolution of fluids approximating the analysed Grasberg vapour with variable initial H_2S and SO_2concentrations (Table 3) were investigated, by simulating a range of chemical reaction paths during cooling.

Thermodynamic data

The selection of species and thermodynamic data for the present study aims at the simplest chemical system that can still convey the essential reaction behaviour of low-salinity to medium-salinity magmatic–hydrothermal fluids, in terms of the mass-balance between major and trace components and the main minerals observed in epithermal ore deposits. A summary of data sources is given in Table 4, and the full dataset is available as a Repository Supplement. Thermodynamic data of Johnson et al. (1992) updated by Sverjensky et al. (1997; SUPCRT95) were used for sulphide, oxide and simple silicate minerals, which for the low-pressure conditions and the simple minerals of interest here provide essentially identical results as those available from Holland and Powell (1998). Complexes of Au, Cu, As and some other key species were replaced by data derived from more recent experiments in a manner ensuring internal consistency.

The solubility of *gold* has recently been re-investigated with a flow-through apparatus yielding high-precision equilibrium concentrations under completely controlled conditions of pressure, temperature, and concentrations of sulphur, acid and hydrogen in the

Table 3 Idealised chemical compositions of medium-salinity magmatic fluids, based on experimental equilibria in the single-phase stability field, and on LA-ICPMS analyses of fluid inclusions from the Grasberg (Irian Jaya) and Butte (Montana) porphyry deposits

Component[a]	Single-phase fluid (mol kg^{-1} H_2O)	Grasberg vapour (mol kg^{-1} H_2O) (by wt)
NaCl	0.8[b]	1.2 (3% Na)[d]
KCl	0.5[b]	0.33 (1.3% K)[d]
$FeCl_2$	0.2[b]	0.18 (1% Fe) [d]
CuCl	0.1[c]	0.19 (1.2% Cu) [d]
$As(OH)_3$		0.003 (200 ppm As)[d]
AuCl		5×10^{-5}(10 ppm Au)[d]
$CaCl_2$[b]	0.04[b]	0.03[b]
HCl	0.02[b]	0.02[b]
H_2S	0.2 ± ??[b]	0.03...0.6[e]
SO_2	0.2 ± ??[b]	0.03...0.6[e]

[a]Components expressed as neutral complexes without implying knowledge of actual speciation
[b]Estimated from fluid–granodiorite equilibration experiments by Burnham (1979) and other considerations discussed in text, for a fluid of similar salinity to the Grasberg vapour
[c]From LA-ICPMS analyses of intermediate-density fluids in porphyry-stage veins from Butte, Montana (Rusk et al. 2004)
[d]From LA-ICPMS analyses of Grasberg vapour inclusions by Ulrich et al. (1999); 7 wt% NaCl equivalent salinity using the microthermometric approximation of Heinrich et al. (2003)
[e]Varied within the indicated ranges in the multicomponent equilibrium calculations summarized in text

system (Stefánsson 2003; Stefánsson and Seward 2003, 2004). These data yielded the first internally consistent set of stability constants for all geologically significant gold complexes in the Au–Cl–S–O–H–Na system at 500 bar, from ambient temperature to 450°C. Additional data cover the small pressure dependence from steam saturation pressure to 1.5 kbar. For this modelling study, Gibbs free energy functions of temperature at 500 bar have been fitted to the experimental equilibrium constants given by Stefánsson (2003) for $AuOH^0$, $AuCl_2^-$, $AuHS^0$ and $Au(HS)_2^-$ and for aqueous HS^-, $NaHS^0$, $NaCl^0$, HCl^0 and H_2^0 to ensure internal consistency. As a result, gold solubilities are the most reliable data in the following predictions.

Copper complexation experiments involving hydroxy, bisulphide and chloride ligands were evaluated by Akinfiev and Zotov (2001) who fitted published experiments to the HKF formulation for extrapolation. The most important copper(I) species in medium-salinity fluids are chloride complexes, whose thermodynamic data were derived from the largely concordant solubility experiments by Xiao et al. (1998) and Zotov et al. (1995) up to 350°C. The complex $CuCl_3^-$ was ignored (cf. Liu et al. 2001), because it is not well-constrained at high temperature; it would probably be significant in hypersaline magmatic liquids, but these are not modelled here. Cu(I) bisulphide data were fitted by Akinfiev and Zotov (2001) to experimental results by Mountain and Seward (1999), and $Cu(HS)_2^-$ indeed contributes significantly to copper transport in sulphide rich, pH-neutral magmatic fluids.

Arsenic is a characteristic component of high-sulphidation epithermal and many other gold deposits. Experiments by Pokrovski et al. (1996) have confirmed earlier predictions (Heinrich and Eadington 1986; Spycher and Reed 1989) that the neutral arsenious acid complex ($H_3AsO_3^0$ or more likely $HAsO_2^0$ according to Iakovleva 2003) is a very stable species at high temperatures. Arsenic sulphide species with uncertain degrees of polymerisation may be important in sulphide-rich fluids especially at low temperatures (e.g. Webster 1990), but only $As_2S_3^0$ was included here, using the data recommended by Pokrovski et al. (1996). No experimental stability data exist for the diagnostic arsenic minerals in epithermal deposits, enargite and tennantite. For this study, the stoichiometric estimation procedure of Craig and Barton (1973) was used to estimate the free energy of Cu_3AsS_4 (enargite) from the simple sulphides AsS realgar (Pokrovski et al. 1996) and CuS covellite (Johnson et al. 1992). The free energy function of $Cu_{12}As_4S_{13}$ (simplified tennantite) was derived from that of enargite and the field-based observation of Einaudi et al. (2003) that the desulphidation equilibrium tennantite + S_2(g) = enargite must be close to the f_{S2} of the equilibrium 5$CuFeS_2$ (chalcopyrite) + S_2(g) = Cu_5FeS_4(bornite) + 4FeS_2 (pyrite). As a result of all these uncertainties, arsenic solubilities calculated in this study are of indicative value only. The simple Cu–As-mineral estimation was preferred over an alternative dataset based on a significantly higher thermodynamic stability of Fe-tennantite as proposed by Seal et al. (1990); if combined with aqueous As species data from Pokrovski et al. (1996) this yields unrealistically low arsenic solubilities at all temperatures.

The remaining aqueous species data from SUPCRT95 are subject to uncertainty, especially for $T > 400$°C at low pressures close to the recommended limit of validity of the HKF equation of state (Johnson et al. 1992). The oxidised aqueous sulphur species, in particular, and the computed sulphur solubility might be in error under these conditions, but this should not seriously affect the gold solubility relationships, which are computed from the internally consistent dataset of Stefánsson (2003) at 500 bar. Aqueous Al species were not considered for simplicity, even though acidic magmatic fluids actively dissolve Al minerals (Fig. 1b). Aqueous Al species would probably replace the stability fields of pyrophyllite and andalusite predicted by some of the higher-temperature results shown below.

Data fitting and reaction modelling were carried out with the ETH-updated version of the CSIRO-Thermodata package (Turnbull and Wadsley 1986; Heinrich et al. 1996), using program CHEMIX for multicomponent–multiphase equilibrium calculations. Activity coefficients for the aqueous phase were computed using the model of Oelkers and Helgeson (1991), with parameters for the Debye–Hückel terms consistent with the complex stability derivations by Stefánsson (2003). No solid solutions were considered in the present calculations. Calculations were carried out for

Table 4 Species and sources of thermodynamic data for parts of the chemical system Na–K–Fe–Ca–Cu–As–Au–H–Cl–S–C–O–H used in this study, applicable at 500 bar and 25–450°C

Species	Data Source
Gases	
O_2 (g)	Turnbull and Wadsley (1986) CPDMRL
S_2 (g)	Turnbull and Wadsley (1986) CPDMRL
N_2 (g)	Turnbull and Wadsley (1986) CPDMRL
H_2 (g)	Turnbull and Wadsley (1986) CPDMRL
A. species	
H_2O liquid	Johnson et al. (1992)
OH^-(aq)	Johnson et al. (1992), update Sverjensky et al. (1997)
H_2 (aq)	Stefánsson (2003)
HCl (aq)	(Ho et al. 2001) as used by Stefánsson (2003)
H^+(aq)	Johnson et al. (1992), update Sverjensky et al. (1997)
NaCl (aq)	Johnson et al. (1992), update Sverjensky et al. (1997)
Na^+(aq)	Johnson et al. (1992), update Sverjensky et al. (1997)
NaOH (aq)	Johnson et al. (1992), update Sverjensky et al. (1997)
KCl (aq)	Johnson et al. (1992), update Sverjensky et al. (1997)
K^+(aq)	Johnson et al. (1992), update Sverjensky et al. (1997)
Cl^-(aq)	Johnson et al. (1992), update Sverjensky et al. (1997)
$CaCl_2$(aq)	Johnson et al. (1992), update Sverjensky et al. (1997)
Ca^{2+}(aq)	Johnson et al. (1992), update Sverjensky et al. (1997)
$CaCl^-$(aq)	Johnson et al. (1992), update Sverjensky et al. (1997)
$CaSO_4$(aq)	Johnson et al. (1992), update Sverjensky et al. (1997)
CuCl (aq)	Akinfiev and Zotov (2001)
$CuCl_2^-$(aq)	Akinfiev and Zotov (2001)
CuHS (aq)	Akinfiev and Zotov (2001)
$Cu(HS)_2^-$(aq)	Akinfiev and Zotov (2001)
CuOH (aq)	Akinfiev and Zotov (2001)
$Cu(OH)_2^-$(aq)	Akinfiev and Zotov (2001)
$FeCl_2$(aq)	Johnson et al. (1992), update Sverjensky et al. (1997)
$FeCl^+$(aq)	Johnson et al. (1992), update Sverjensky et al. (1997)
Fe^{2+}(aq)	Johnson et al. (1992), update Sverjensky et al. (1997)
H_2S (aq)	Johnson et al. (1992), update Sverjensky et al. (1997)
HS^-(aq)	Stefánsson (2003)
NaHS (aq)	Stefánsson (2003)
SO_2(aq)	Johnson et al. (1992), update Sverjensky et al. (1997)
HSO_3^-(aq)	Johnson et al. (1992), update Sverjensky et al. (1997)
SO_3^{2-}(aq)	Johnson et al. (1992), update Sverjensky et al. (1997)
HSO_4^-(aq)	Johnson et al. (1992), update Sverjensky et al. (1997)
$NaSO_4^-$(aq)	Estimated from SUPCRT95 (Johnson et al. 1992) assuming $NaSO_4^-$(aq) = KSO_4^-(aq)–NaCl (aq) + KC l(aq)
KSO_4^-(aq)	Johnson et al. (1992), update Sverjensky et al. (1997)
SO_4^{2-}(aq)	Johnson et al. (1992), update Sverjensky et al. (1997)
SiO_2(aq)	Johnson et al. (1992), update Sverjensky et al. (1997)
$As(OH)_3$(aq)	Pokrovski et al. (1996)
As_2S_3(aq)	Pokrovski et al. (1996)
AuHS (aq)	Stefánsson (2003)
$Au(HS)_2^-$(aq)	Stefánsson (2003)
$AuCl_2^-$(aq)	Stefánsson (2003)
AuOH (aq)	Stefánsson (2003)
Solids	
$KAlSi_3O_8$(ksp)	Johnson et al. (1992)
$NaAlSi_3O_8$(ab)	Johnson et al. (1992)
$KAl_3Si_3O_{10}(OH)_2$(mus)	Johnson et al. (1992)
$Al_2Si_2O_5(OH)_4$(kao)	Johnson et al. (1992)
$Al_2Si_4O_{10}(OH)_2$(pyp)	Johnson et al. (1992)
Al_2SiO_5(and)	Johnson et al. (1992)
SiO_2(qz)	Johnson et al. (1992)
AlOOH (dsp)	Johnson et al. (1992)
$KAl_3S_2O_{14}H_6$(alu)	Stoffregen et al. (2000)
$CaSO_4$(anh)	Johnson et al. (1992)
$CaCO_3$(clc)	Johnson et al. (1992)
$Ca_2Al_3Si_3O_{12}(OH)$ (clz)	Johnson et al. (1992)
$CuFeS_2$(cpy)	Johnson et al. (1992)
Cu_5FeS_4(bn)	Johnson et al. (1992)
CuS (cv)	Johnson et al. (1992)
Cu_2S (cc)	Johnson et al. (1992)
FeS_2(py)	Johnson et al. (1992)
FeS (po)	Johnson et al. (1992)
Fe_3O_4(mt)	Johnson et al. (1992)

Table 4 (Contd.)

Species	Data Source
Fe_2O_3(hem)	Johnson et al. (1992)
FeO (1) ("FeO")	Proxy "FeO" for "rock redox buffer" of Giggenbach (1992), such that log $R_H = \log f_{H2}/f_{H2O} = -2.8$ in equilibrium with Fe_3O_4 + "FeO"; fumarole gas equilibria updated by Einaudi et al. 2003)
Au (gold)	Turnbull and Wadsley (1986) CPDMRL
S (S)	Turnbull and Wadsley (1986) CPDMRL
Cu_3AsS_4(ena)	Estimated based on simple sulphides from Johnson et al. (1992) using method of Craig and Barton (1973)
$Cu_{12}As_4S_{13}$(ten)	Based on field observation (Einaudi et al. 2003) indicating that equilibrium ena = ten + S_2 (g) must be close to bn + py = cpy + S_2 (g), using estimated data for enargite
$Na_{1.04}K_{0.85}Ca_{0.61}Fe^{II}_{0.31}Fe^{III}_{0.26}Al_{3.11}Si_{11.51}O_{29.94}$	Idealised composition of Early-P3 dacite porphyry (Ulrich and Heinrich 2001; sample 43–47.1/580 m) representing correct total iron, redox and acid exchange capacities, normalised to 1 kg/formula unit

Full data set in a format consistent with the ETH-modified CSIRO-Thermodata package is available upon request from heinrich@erdw.ethz.ch

temperatures between 150°C and 450°C at pressures between the boiling curve and 500 bar. All results shown below apply to 500 bar, where the most complete set of experimental thermodynamic data is available for aqueous liquids of low to intermediate salinity. At temperatures below 350°C, all results were found to be insensitive to pressure variations between 500 bar and the steam saturation curve (see Hemley et al. 1992).

Four endmember reaction pathways for cooling magmatic fluids

Multicomponent equilibrium calculations in homogeneous and heterogeneous systems were carried out to explore the chemical evolution of medium-salinity fluids during isobaric cooling to an aqueous liquid, testing the fluid-compositional ranges shown in Table 3 for a large number of reaction scenarios. The results of such calculations are primarily constrained by the relative concentrations in the input fluid. All of the results shown below therefore refer to a single salinity of 7 wt%, taking the analysed metal concentration ratios of the Grasberg fluid as a starting point (Table 3). In an initial set of models illustrated by Fig. 4, wall rock interactions were reduced to Na–K–H–Al-silicates, to explore the general reaction relationships affecting metal transport. Of key interest is the influence of the initial concentrations of sulphur species, and the effects of mineral reactions affecting the acid/base balance and the pH of the fluid with decreasing temperatures. The total acid content of the vapour-derived fluid is dominated by the contribution to acidity by reactions among sulphur species and a smaller contribution from HCl.

Variations in the initial concentrations of H_2S and SO_2 have a decisive influence on the chemical evolution of magmatic–hydrothermal fluids during cooling, as shown in Fig. 4 by four sets of calculations illustrating four extreme cases of reaction behaviour. Each of the four parts of Fig. 4depicts a series of heterogeneous equilibrium states (fluid + minerals) computed for a closed system at different temperatures between 450°C and 150°C. Aqueous species concentrations in the fluid at equilibrium are shown in each of the upper diagrams, coexisting mineral species are shown in the smaller plots below. Results at each temperature depict the state of a fluid + mineral system assuming direct transfer of the model fluid to the temperature of interest. Two sets of assumptions regarding the relative concentrations of sulphur (H_2S, SO_2) and chalcophile metals (Cu, Fe) are contrasted between the upper (Figs. 4a, c) and lower rows (Figs. 4b, d) in the figure. Both sets are computed for two assumptions regarding acid/base control—either dominated by internal fluid equilibria in the left column of the figure, or assuming pH buffering by excess feldspars in the right column.

Figure 4a shows the predicted equilibrium states in a system in which the molal concentrations of Cu and Fe exceed those of both H_2S and SO_2, and in which acid-base equilibria are dominated by reactions among S–Cl–O–H species within the fluid. Only a small amount of Al silicate is added, to monitor the stable assemblages among kaolinite, pyrophyllite, andalusite and alunite with excess quartz. Because of bornite and pyrite saturation between 250°C and 400°C, the initially modest H_2S concentration is further depleted with falling temperature, by reaction with excess Fe and Cu in the fluid. Acidity ($HCl + H^+$) is high and increases with falling temperature, because of the acid-producing disproportionation of SO_2 to sulphide and sulphate (Giggenbach 1980, 1992):

$$4SO_2 + 4H_2O = H_2S + 3HSO_4^- + 3H^+$$

and the lack of any effective H^+ sink in this set of assumptions. Low reduced sulphur and high acid activity cause 90–99% of the initial high gold concentration in the fluid to precipitate at any reaction temperature, with a little $AuHS^0$ and $AuCl_2^-$ remaining in

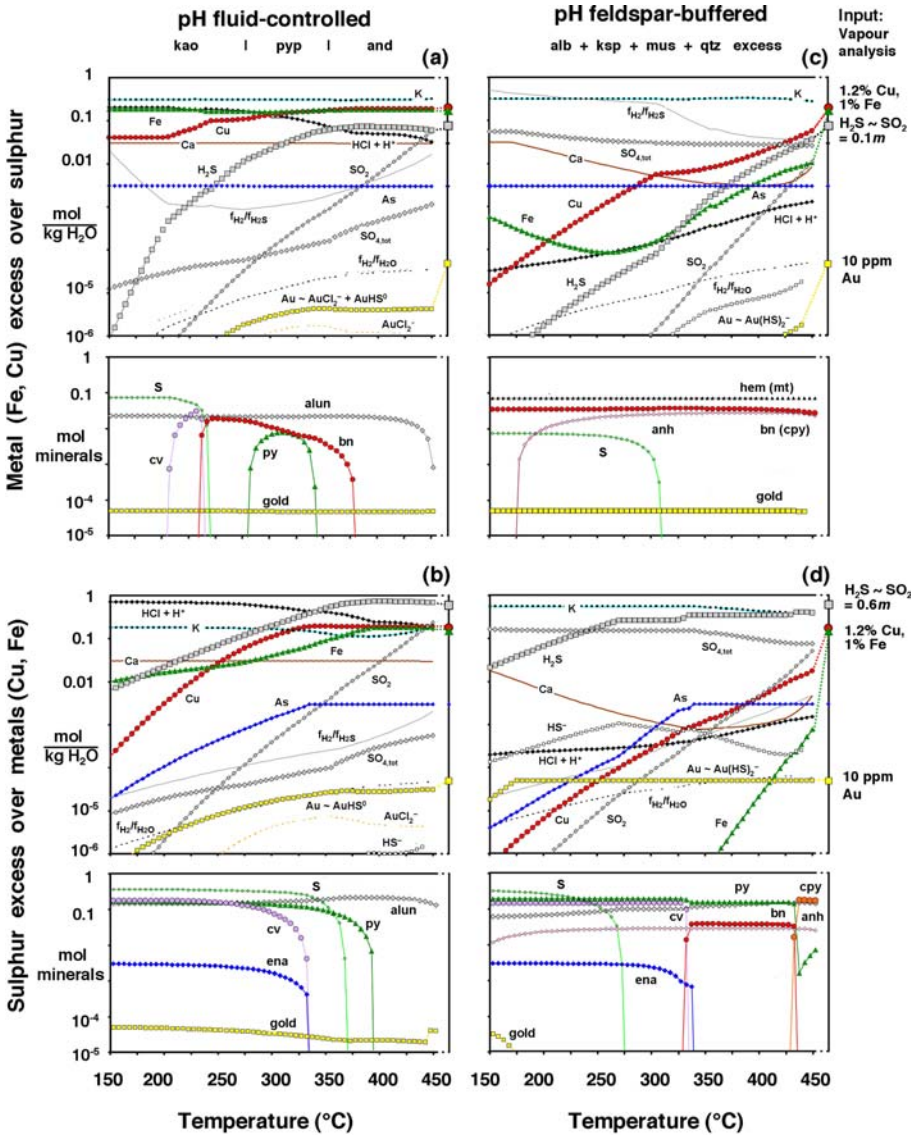

Fig. 4 Results of multicomponent reaction modelling for single-step rock-buffered and fluid-dominated cooling of an intermediate-salinity fluid with high Cu, As and Au content, idealised from LA-ICPMS microanalyses of vapour-like fluid inclusions in the Grasberg porphyry-Cu–Au deposit (Ulrich et al. 1999, Table 3). Four extreme fluid evolution paths are compared, as defined by two sets of limiting assumptions. The *left column* assumes fluid-dominated acid–base balance in which pH is controlled by internal equilibria among dissolved species (models **a** and **b**), whereas the right column assumes feldspar-buffered acid-base conditions (excess K-feldspar + albite + muscovite + quartz; **c**, **d**). sulphur is not analysed by LA-ICPMS, and the concentrations of S species relative to Cu + Fe constitute the main variable in the input fluid composition explored in the upper and the lower two calculations: H_2S and SO_2 deficit relative to the analysed Cu + Fe concentrations (**a**, **c**; *top*) is compared with excess of both sulphur species relative to the metals (**b**, **d**, *below*). Dramatically different gold solubilities as a function of temperature result from these four limiting input assumptions, as discussed in the text

solution. Although such a fluid may cause effective advanced argillic alteration at low temperature, it does not provide optimum conditions for gold transfer to the epithermal environment.

Figure 4b (lower left panel) uses the same assumptions regarding pH balance, but considers an initial excess of H_2S and SO_2 over Fe and Cu. The high sulphide activity causes pyrite saturation already at high temperature, joined by condensed sulphur, covellite and enargite with decreasing temperature. As Cu and Fe are gradually precipitated, the initial sulphide excess cannot be exhausted by mineral precipitation, leading to higher gold concentrations in the fluid compared with the case shown in Fig. 4a, in excess of 1 ppm as $AuHS^0$ at all temperatures down to 200°C.

Figure 4c shows that the effect of sulphide:metal mass balance becomes even more pronounced when acid neutralisation by reaction of the fluid with feldspars (albite + K-feldspar in this model) is permitted. Even a slight initial excess of Fe and Cu over H_2S leads to depletion of the fluid in reduced sulphur, because of the rapidly falling solubility of Cu–Fe sulphides and Fe oxides in near-neutral solutions buffered by K-feldspar + albite + H^+ = muscovite + quartz + K^+ + Na^+ (Hemley et al. 1992). Which of the Cu–Fe minerals (cpy, bn, py, mt and/or hem) saturates first is sensitive to variations in input concentration ratios of Cu:Fe, and the SO_2:H_2S ratio controlling the redox potential of the system. In all cases, however, depletion of sulphide at near-neutral pH leads to very low gold solubilities, preventing efficient transport to epithermal conditions.

Figure 4d illustrates the final case of sulphide excess over metals in a system equilibrated with the feldspar–muscovite–quartz buffer neutralising the pH of the cooling solution. Despite the precipitation of iron rich sulphide assemblages (chalcopyrite + pyrite, followed by bornite + pyrite and finally by covellite + enargite + sulphur + pyrite with falling temperature), even a small

initial excess of H_2S leads to Cu and Fe depletion but high reduced sulphur activity under all conditions. An oxidised fluid with sulphide∼sulphate, and with near-neutral pH maximising HS^-/H_2S, supports maximum gold solubility as $Au(HS)_2^-$. As a result, the initial gold concentration of 10 ppm in the model fluid can be maintained, and extremely high gold contents can be transported without gold saturation down to epithermal temperatures as low as 150°C.

Fluid evolution in calc-alkaline magmatic rocks

Figure 4 illustrates how the chemical behaviour of an intermediate-salinity fluid critically depends, especially with regard to gold transport, on relatively small differences in starting fluid composition and assumptions about reaction pathways during cooling. These extreme model cases will not be realised by actual fluids cooling in a porphyry–epithermal system hosted by typical magmatic rocks, because wall rock reactions and mineral precipitation occur progressively during fluid cooling. More importantly, intermediate calc-alkaline rocks also contain a significant fraction of iron, in addition to feldspars and other less-decisive components. FeO in the rock tends to reduce SO_2 to H_2S with falling temperature (Giggenbach 1992; Einaudi et al. 2003), which would enhance gold transport. On the other hand, iron in the wall rocks acts as a sink for sulphide by precipitation of additional pyrite ± pyrrhotite, which reduces gold solubility as sulphide complexes.

To test the net consequence of these counteracting factors, a range of titration experiments (Helgeson 1970) were computed for an idealised fresh dacite composition from the Bajo de la Alumbrera porphyry–Cu–Au system (Ulrich and Heinrich 2001, Table 4), which has FeO and Fe_2O_3 contents typical for intermediate calc-alkaline magmatic rocks. A simplified set of Ca and Fe-bearing mineral species are included to capture the essence of mass-balance without introducing unnecessary complexity due to silicate solid solutions in the natural system (Fig. 5). Results of isothermal equilibration between variable proportions of sulphide-rich fluid and dacite as shown in Figs. 5a, b are similar for all temperatures (except for changes in stable Al silicates: kaolinite, pyrophyllite or andalusite) and for a wide range of input fluid compositions (mainly affecting the type of Fe-oxides and Cu–Fe-sulphides). At high rock/fluid ratios (rock-dominated conditions, right side of Figs. 5a, b), the stable mineral assemblage includes feldspars + muscovite + clinozoisite + Fe oxides + minor pyrite, chalcopyrite and anhydrite, approximating propylitic alteration assemblages in nature. The coexisting fluid is essentially depleted in sulphide, even if its initial H_2S concentration greatly exceeds that of the chalcophile metals. At moderately high rock/fluid ratios near 0.5 the concentration of H_2S is minimised and the Fe content of the equilibrated fluid exceeds that of all sulphur species, because the total contribution of iron by the rock exceeds that of sulphide contributed even by an initially S-rich fluid. Gold solubility under these conditions is minimal because the effect of pH neutralisation (enhanced HS^-/H_2S) is outweighed by the effect of sulphur depletion of the fluid by wall rock iron reacting to pyrite. Better conditions for high gold solubility for fluids with excess initial H_2S at high temperatures are realised with moderate to low rock/fluid ratios in equilibrium with quartz + Al silicates + alunite ± muscovite ± anhydrite (left half of Figs. 5a, b).

Fluid-rock titration and cooling models discussed so far are simplified closed-system calculations, but they correctly illustrate the wide range of chemically distinct fluid evolution paths that may be taken by natural intermediate-salinity to low-salinity fluids in porphyry–epithermal systems undergoing variable degrees of rock interaction while cooling. Depending on the degree of fluid channelling and the temperature distribution in the natural fluid-flow system, natural fluids will depart from points of partial rock-buffering and subsequently cool in contact with already partially altered rock. To illustrate this variation, four possible cooling and reaction pathways are calculated in the lower half of Figs. 5c–5f. All calculations assume that the Grasberg-like fluid with initial sulphide excess is first equilibrated with variable proportions of model dacite as shown in Figs. 5a, b at 420°C, and then cools in equilibrium with an excess of the ambient mineral assemblage, which is geologically more realistic than direct transfer of magmatic vapour to epithermal conditions. The evolving fluid compositions as a function of temperature are plotted for four cases in Figs. 5c–5f, and the resulting mineral assemblages and inferred geological processes are shown below each diagram.

Figure 5c approximates an evolution that will result from strong focussing of the fluid at high temperature, such that the fluid is saturated with quartz and alunite only (e.g., a vuggy quartz zone). This leads to an acid, Fe-rich and As-rich fluid at low temperatures, with declining sulphur content due to elemental sulphur condensation but relatively high Cu and Au content (as $AuHS^0$), because of the high acidity of the fluid. Such a fluid will actively promote acid leaching with falling temperature. Gold ± enargite mineralisation may occur, most likely in low-grade disseminated form, because of the gradual decrease of gold solubility with falling temperature.

A fluid departing from high-temperature rock interaction within the stability field of aluminosilicates, alunite and/or anhydrite is shown in Fig. 5d. This case exemplifies a magmatic fluid focussed into a zone of argillic (or pyrophyllite/andalusite) to phyllic alteration at high temperature, prior to exhaustion of dissolved sulphide by iron in the wall rock. This fluid will cool with continued pyrite + Cu–Fe sulphide and later with pyrite + covellite + enargite precipitation. Much of the high initial sulphide content can be maintained under these conditions, allowing almost temperature-independent gold solubilities in excess of 2 ppm. Evolution

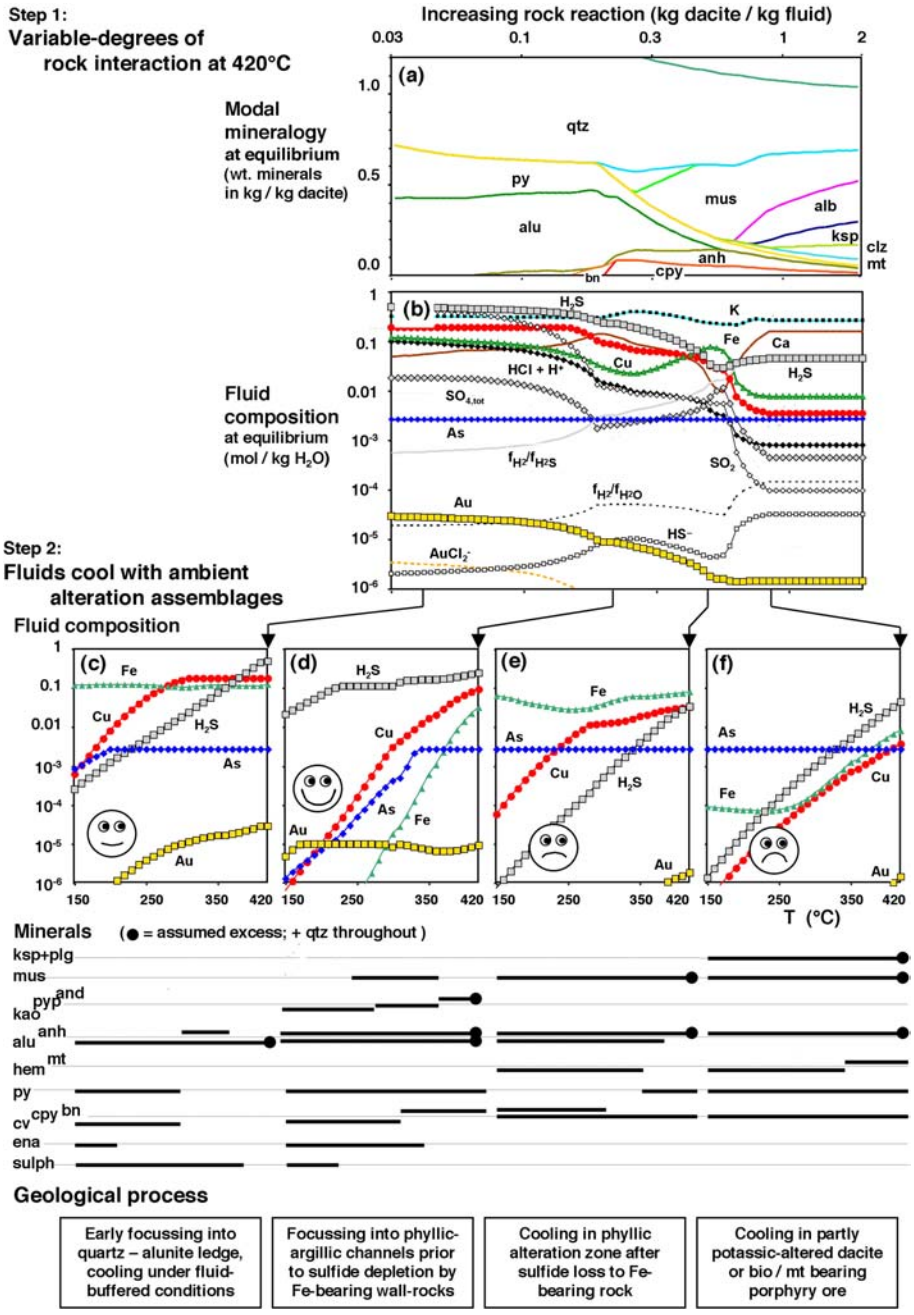

Fig. 5 Isothermal titration plot illustrating the additional effects of iron in intermediate-composition igneous wall rocks during high-temperature wall rock interaction (**a**, **b**: model step 1 calculated for 420°C), and four fluid evolution paths representing different degrees of wall rock interaction during subsequent cooling to epithermal conditions (step 2: **c**–**f**). With increasing rock reaction (**a**, **b**), sulphur in the fluid is consumed by reaction with Fe from the rock to form pyrite, leading to sulphur depletion and gold precipitation in dispersed form. In nature, fluids become variably channelled into veins during cooling, which lead to a range of chemical evolution paths represented by (**c**–**f**). The calculations in the *lower row* of the diagrams assume that the fluid departs from variably altered porphyry at 420°C, as indicated by *arrows* linking four fluid compositions in (**b**) to the high-temperature starting points of the four diagrams (**c**–**f**). Subsequent cooling of each fluid assumes contact with the ambient, partially altered rock. Resulting mineral assemblages are shown *below* each fluid evolution diagram. The entire spectrum of predicted processes indeed occurs in porphyry–epithermal systems, but gold transport to low temperature is most efficient in a fluid whose initial H_2S excess over Cu + Fe is partly maintained, by fluid cooling in a vein zone with complete wall rock sulphidation permitting mildly acid conditions near the sericite–aluminosilicate equilibrium (**d**)

paths approximating this model are predicted to be the most effective for transporting gold into the epithermal realm, because they allow high gold concentration in the fluids without gradual dispersion along the flow path. Slight gold under-saturation between 300°C and 180°C even permits local redissolution and "zone refining" along the flow path. High-grade gold precipitation can occur at any temperature as low as 180°C, if sudden fluid-compositional changes are imposed by a change in local geological environment.

Fluid evolution paths undergoing greater degrees of reaction with magmatic rocks at high temperature, followed by cooling in contact with phyllic ± feldspar-bearing assemblages are likely to become depleted in sulphide due to the Fe contribution from the wall rocks, as shown for two cases in Figs. 5e, f. Cooling of a fluid in a phyllic alteration zone after sulphide depletion is likely to cause precipitation of most Cu and Au at temperatures above 350°C, for example, in the feldspar-destructive top of a shallow porphyry deposit. The resulting lower-temperature fluid may still contain appreciable Cu and As, but little Au. Figure 5f involves a high-degree of rock reaction, leading to complete trapping of all ore metals (except As) in a partially altered igneous rock. Processes represented by Figs. 5e, f will contribute to porphyry-style Cu–Au mineralisation,

but are not conducive to gold transport down to epithermal temperatures.

"Telescoping" by downward retraction of isotherms during continued magmatic fluid flow

Geological processes leading to all of the chemical evolution paths predicted by Figs. 5c, f are widespread in calc-alkaline magmatic–hydrothermal systems and observed to follow a systematic pattern in space and time. Published field observations summarized above (Table 1, Fig. 1) indicate that fluid evolution paths departing from various degrees of wall rock buffering succeed each other in a typical sequence, as a result of progressive cooling of a subvolcanic porphyry stock above a larger intrusion of hydrous magma. Downward retraction of a magmatic interface and surrounding isotherms during continued fluid exsolution from a magma reservoir explains the characteristic paragenetic sequence of high-sulphidation gold deposits, their spatial and sometimes temporal association with variably mineralised porphyry systems, and the widespread overprinting of early potassic by later phyllic alteration seen in many porphyry-style ore deposits (Fig. 1; Heinrich et al. 2004, Fig. 3).

At an early stage, after the emplacement of a porphyry stock above a cupola in the roof of a larger subvolcanic magma chamber (Fig. 1a), exsolution of magmatic volatiles will start in the uppermost part of the crystallising magma column, possibly fed at this early stage by convection of hydrous magma through the still largely molten stock (Shinohara et al. 1995). Initially, volatiles will exsolve from the magma at relatively low pressure and will therefore commonly be in the two-phase fluid stability field, with vapour greatly predominating over hypersaline liquid or even solid halite. The highly acid vapour phase will be expelled by hydraulic fracturing and ascend (with or without entraining some of the heavier liquid phase) along a relatively short flow path across an initially very steep pressure and temperature gradient. Such conditions favour the injection of acid fumarolic vapour into structurally controlled fluid conduits. Mixing with groundwater subsequently leads to intense argillic alteration and the formation of initially barren vuggy-silica (Fig. 1b). These acid fluids generallly contain not much gold because of their very low density (Hedenquist et al. 1993; see Williams-Jones et al. 2002), or they may lose any initial gold content close to the magmatic interface.

As cooling of the stock progresses, the magma crystallisation front will retract downward, temperature gradients will attenuate, and the upper part of the system will cool. Its temperature structure will be a complex function of the rate of magmatic fluid supply, the mode and degree of phase separation, and the rate of conductive heat loss to the surrounding rocks, which may be cooled by externally convecting meteoric water. Continued fluid exsolution from the magma will occur at progressively greater depth and higher pressures, and may initiate the formation of porphyry-style ores from variable proportions of hypersaline liquid and vapour (Fig. 1a). Two-phase fluid conditions may be attained either by boiling of an initially single-phase liquid (Ulrich et al. 2001) or by condensation of saline liquid from an initially single-phase vapour (Redmond et al. 2004). The mode of phase separation depends on the *P–T* conditions where the two-phase surface is breached and on the water:salt ratio of the incoming single-phase fluid (Fig. 3), which in turn may vary as a function of the depth and degree of crystallisation of the source pluton (Cline and Bodnar 1991). High-temperature Cu–Au precipitation in the porphyry regime will be aided by cooling of the magmatic fluids and reaction with initial Fe in the wall rocks (Fig. 5e or 5f).

With further cooling of the entire magmatic system, the zones of potassic alteration and Cu–Fe sulphide (± gold) precipitation in the gradually forming porphyry deposit expand downward, with potassic alteration initiated at higher temperature closer to the magmatic interface and Cu–Fe sulphide and gold precipitation between 420°C and 350°C somewhat higher up (Ulrich et al. 2001; Landtwing et al. 2004). Successively higher pressure attending fluid exsolution at increasing depths in an overall cooling system will favour *P–T* paths allowing the vapour to contract to liquid during ascent (Fig. 3), compared with the early stage of low-density vapour emanation from the top of the porphyry. At the same time, any hot and relatively dense vapour preferentially escaping form the deepening two-phase zone will be forced to pass through an increasing thickness of feldspar-rich rock, including the hydrothermal K-feldspar generated by potassic alteration with partial or complete sulphidation to Cu–Fe sulphide ore. Given any pressure–temperature path that remains in the single-phase field during ascent from the deepening region of phase separation (Fig. 3), the vapour-derived fluid may depart from the chemical rock buffer at any point before complete de-sulphidation by Fe in the wall rocks. These conditions, captured approximately by the instantaneous isotherm distribution indicated in Fig. 1a, are ideal for a physical and chemical reaction path similar to that modelled in Fig. 5d, which is the most favourable for transporting sulphide-complexed gold to lower temperature.

Fracture zones with quartz + pyrite ± chalcopyrite surrounded by exhaustive feldspar-destructive alteration (kaolinite/pyrophyllite/andalusite ± muscovite ± sulphates) are the preferred channelways for such gold-transporting, vapour-derived liquids. Such structurally controlled and often upward-flaring alteration zones commonly overprint potassic alteration and copper mineralisation in the roofs of porphyry deposits (e.g. Sillitoe 1973; Gustafson and Hunt 1975; Hedenquist et al. 1998; Perello et al. 2001; Ulrich and Heinrich 2001; Watanabe and Hedenquist 2001; Fig. 1c). Erosion or sector-collapse of a volcanic edifice may further contribute to this "telescoping" of superimposed alteration

types, reducing their depth range by gradual or instantaneous increase in pressure and temperature gradients (Sillitoe 1994). Removal of overburden will steepen the gradients of chemical disequilibrium (e.g. by sudden boiling) and may thus favour localised gold precipitation from contracted vapour fluids of high initial gold content.

Application to selected epithermal ore systems

The "isotherm retraction–vapour contraction" model proposed in Heinrich et al. (2004) and tested with the model calculations shown in Figs. 4 and 5rationalises recurrent observations in porphyry–epithermal ore systems in terms of general fluid chemistry and physics. More specifically, the range of model evolution paths shown in Figs. 3, 4, and 5 also provide a basis for explaining individual features in some of the best-described Cu–As–Au ore systems.

At *El Indio*, studied in detail by Jannas et al. (1990), an early paragenesis of pyrite–enargite with comparatively modest gold grade was deposited by moderately saline fluids (3–4 wt% NaCl eq) at temperatures of 220–280°C. These copper-rich veins predominate in the deeper parts of the mine, and enargite precipitation followed after advanced argillic alteration with abundant alunite. Ore-forming fluids entering the vein system at this stage are most consistent with a deeper fluid history of intense wall rock reaction approximated by the model calculation of Fig. 5e, providing mildly acid Cu and As-rich solutions ascending to the deposit level after initial pre-ore acid leaching. The famous bonanza-grade gold veins cut and overprint the enargite veins and were formed at largely overlapping temperatures (190–250°C) by less saline fluids (~1.4 wt% NaCl eq) in the pH stability field of muscovite/illite + kaolinite + quartz. Neither of the two ore stages show clear fluid mixing trends towards meteoric fresh water, but a tennatite-rich transition stage records fluid inclusions of intermediate salinity that may represent mixtures of the two ore fluids (Jannas et al. 1990, p. 270). The decrease in fluid salinity from 3–4 to 1.4 wt% could result from the separation of vapour from a hypersaline liquid at depth, at slightly decreasing pressure over time (Fig. 3). If the lower-salinity vapour ascended along the flow paths that had already been altered and sulphidised by the earlier higher-salinity fluid, it would maintain its high initial sulphide content for effective gold transport, approximating the model evolution paths of Figs. 4d or 5d. Mixing of some earlier, already Cu-depleted but still As and Fe-rich fluid with the slightly later Au and S-rich fluid would provide a very efficient mechanism for high-grade gold precipitation with quartz + pyrite + tennatite + chalcopyrite, in localised structures at any depth in the deposit and without boiling (Jannas et al. 1990). A similar interpretation may apply to the Pepa vein as one of the smaller but exceptionally high-grade gold deposits in the Maricunga district (Muntean and Einaudi 2001).

The *Far South East (FSE)—Lepanto* system in the Philippines is probably the best-documented association of nearly coeval porphyry-style and high-sulphidation epithermal ore deposits (Arribas et al. 1995b; Hedenquist et al. 1998; Claveria 2001). Medium-salinity aqueous fluids (1–7 wt%) deposited quartz + pyrite + chalcopyrite + gold in veins with phyllic alteration haloes at T~325°C, overprinting earlier largely barren quartz stockwork veins associated with higher-temperature potassic alteration in the FSE porphyry (Hedenquist et al. 1998). This porphyry deposit contains a much greater total copper and gold resource than the associated high-sulphidation veins of the Lepanto mine, which has an overall similar Cu/Au ratio but locally much higher gold grades and contains most of the copper in Cu–As sulphides (Hedenquist et al. 1998). Low-salinity fluids similar to those in the quartz-pyrite-chalcopyrite veins of the porphyry also represent the hot endpoint of the epithermal mixing trend towards cool meteoric water, determined mainly from enargite-hosted fluid inclusions (Fig. 2d; Mancano and Campbell 1995). The paragenetic sequence at Lepanto involves early advanced argillic alteration and vuggy quartz leaching, followed by enargite/luzonite + pyrite, and then chalcopyrite + tennatite. A final phase of gold introduction commonly with covellite + pyrite indicates a late flux of gold-rich fluid at low temperature but very high sulphide activity (Claveria 2001).

The zoning and paragenetic sequence in the FSE–Lepanto system matches almost exactly the superposition of reaction pathways as shown by Figs. 5d–5f. After initial advanced argillic alteration by low-density vapour ascending from shallow but high-temperature potassic alteration, isotherms retracted and the porphyry was mineralised by contracting vapour that may have originated as a single-phase fluid (Hedenquist et al. 1998), but more likely attained an essential excess of S over Fe by separation from hypersaline liquid at greater depth. The subsequent zoning and deposition sequence of different sulphides and gold can be explained by continued input of a low-salinity vapour-derived fluid with essentially constant composition but successively increasing degree of fluid focussing while the system as a whole was cooling and isotherms were retracting to greater depth. Cu–Au mineralisation in the porphyry formed by intimate interaction with the wall rock, leading to partial phyllic alteration and Cu–Fe sulphide precipitation to the point of sulphide exhaustion, thereby co-precipitating gold and copper in proportions approximating the initial metal ratio in the fluid, as modelled in Fig. 5f. Subsequent batches of similar fluid focussed through the same structures would have an increasing chance of maintaining some sulphide, and Cu and As, as predicted by Fig. 5e, enabling precipitation of enargite in the overlying epithermal veins at temperatures below 280°C. Chalcopyrite + tennantite deposition will occur as the fluid progressively becomes depleted in sulphur by sulphide precipitation (not modelled; see Einaudi et al. 2003). Further cooling of the final batches of similar

low-salinity fluid under increasingly fluid-dominated conditions, because of increasing amounts of structural fluid focussing and shielding from Fe-bearing wall rocks, will enable optimum gold-only transport down to temperatures as low as 150°C (the minimum recorded by Mancano and Campbell 1995), as modelled in Fig. 5d.

Carbonate buffering and the formation of Carlin-type gold deposits

Despite their different geological setting in carbonate-bearing sedimentary host rocks, Carlin-type gold deposits may have a related origin in terms of fluid-chemical evolution. They share a similar element-enrichment pattern with high-sulphidation epithermal deposits (S, As, Te, Sb, Bi, Tl and Hg, besides Au and Ag; Kesler et al. 2003b) and are formed at the low-temperature end of the epithermal spectrum (~150–230°C) from variably CO_2-rich fluids with salinities in the same characteristic range of 3–9 wt% NaCl equivalent (Cline and Hofstra 2000; Emsbo et al. 2003). The ore-transporting fluids are moderately acid, with kaolinite alteration in zones of strong fluid focussing where carbonates are completely dissolved (Cail and Cline 2001; Emsbo et al. 2003). The generation of secondary pervasive permeability and porosity by carbonate dissolution from marly mudstones and sandstones is a characteristic of the formation of these grossly stratabound, and typically rich and large-tonnage gold orebodies. Sillitoe and Bonham (1990) proposed a magmatic–hydrothermal fluid source possibly related to porphyry–Cu–Au mineralisation in some districts. A dominant component of rock-equilibrated meteoric fluid is favoured by some authors (Emsbo et al. 2003), but this does not exclude a major or dominant contribution of As and Au from a deep low-salinity magmatic or metamorphic fluid component (Kesler et al. 2003b; Johnston and Ressel 2004).

Reaction with carbonate-bearing sedimentary rocks is an excellent alternative to acid neutralisation by feldspar alteration, to maintain a sulphide-rich fluid at near-neutral pH conditions over a long transport path from a distal magmatic source to the low-temperature deposits. Compared with calc-alkaline magmatic rocks, marly mudstones and sandstones are richer in carbonate and Al silicates (depending on the component of immature clastic material) but have much lower total iron contents. Such sedimentary rocks thus have greater pH buffering capacity, but a lower capacity for de-sulphidising an H_2S-rich fluid. These are conditions that will optimise gold transport to an extent that cannot be easily realised by cooling of a magmatic fluid in contact with igneous rocks (Fig. 5). Figure 6predicts the evolution of the same vapour-derived magmatic fluid (Table 3) assuming initial excess of H_2S over ore metals, but cooling in contact with a limited quantity of a model mudstone containing equal proportions of calcite, quartz, and muscovite (~illite). At high temperature, this model predicts skarn-like assemblages represented simplistically by anhydrite + clinozoisite + potassium feldspar + quartz + chalcopyrite + bornite. High-temperature Cu–Fe-sulphide precipitation, and saturation with calcite + muscovite and high-sulphidation Cu–As minerals at intermediate temperatures, will tend to partly deplete a medium-salinity magmatic fluid in these elements; but pH neutralisation at sustained high-sulphide content will maintain gold under-saturation and transport at very high concentrations (10 ppm) at any temperature. The physical process generating permeability for far-field flow of ore fluids by rock decarbonation, and the chemical process of maintaining optimum gold transporting conditions by an H_2S-rich magmatic fluid, thus mutually enhance each other and could be a key to the genesis of rich Carlin-type gold deposits. The proposed magmatic–hydrothermal fluid source can be located at greater depth than that of most porphyry-Cu–Au deposits, because CO_2, will widen the two-phase region compared with the binary H_2O–NaCl system and allow liquid–vapour separation even in the deeper parts of the crust.

Figure 6 is a closed-system cooling model reducing the extended fluid pathways typical for Carlin-type gold systems to a single reaction step. More realistically, stepwise chemical reaction of a cooling and contracting magmatic vapour with carbonate-rich sedimentary rocks will produce a Cu-depleted, but arsenic, sulphur and gold-rich solution at low temperature (Fig. 6). Despite its high gold concentration, the resulting low-temperature ore fluid is undersaturated in metallic gold, consistent with mineralogical evidence for gold deposition in arsenious pyrite solid-solution rather than as native metal, as a result of fluid desulphidation by reaction with iron derived directly or indirectly from the host rocks (Kesler et al. 2003a). This precipitation process has been modelled previously by Woitsekhowskaya and Peters (1998), but the much higher initial Au and As concentrations permitted by a magmatic vapour source would lead to correspondingly higher final ore grade.

Summary and conclusions

Published geological observations, experimental thermodynamic data, and quantitative fluid inclusion microanalyses together delimit the fluid processes that optimise the chances of forming an economic, low-temperature magmatic–hydrothermal gold deposit. High gold concentrations—at ppm levels, as recorded by high-temperature low-salinity to medium-salinity fluid inclusions, and orders of magnitude higher than those previously considered as adequate for ore formation—can be transported without dispersion along the fluid pathway, down to temperatures of ore deposition as low as 150°C. To enable such efficient metal transport, a specific set of physical and chemical conditions for the fluid evolution path between magmatic source and ore deposition site are required.

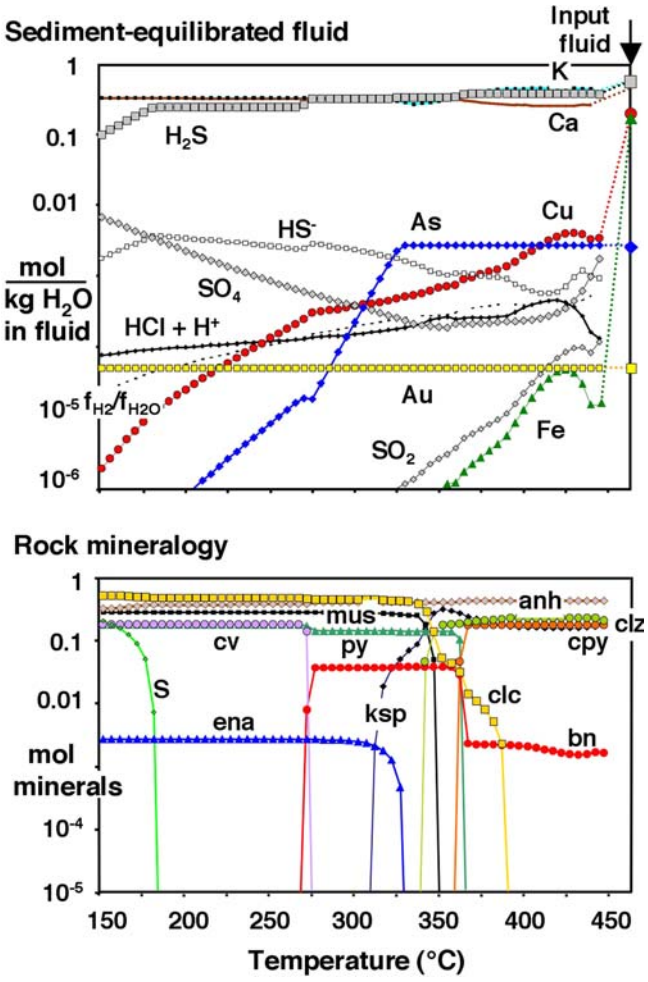

Fig. 6 Cooling of a sulphide-rich fluid in contact with a carbonate-rich mudstone sediment, illustrating that contracted magmatic vapour would be an excellent ore fluid for the generation of Carlin-type gold deposits. Because of the low Fe-content of carbonate-rich sediments relative to their high acid-buffering capacity, 10 ppm Au solubility can be maintained down to temperatures as low as 150°C. Permeability generation by carbonate dissolution and the resulting acid neutralisation may enhance each other, to enable long-distance gold transport from a deep magmatic vapour source to a site of Carlin-type gold mineralisation. Diagram calculated for 1 kg of the same input fluid as used in Figs. 4b, d, equilibrated with 0.1 kg of rock containing equal weight fractions of calcite, muscovite (~illite) and quartz. This single-step calculation differs from geological reality, where most Cu will be precipitated in the high-temperature "skarn" (represented by clinozoisite + anhydrite + chalcopyrite + bornite), so that the cool distal fluid will be depleted in Cu. This will suppress covellite and enargite precipitation, preserving high Au and As concentration for the formation of gold-rich arsenious pyrite

1. *Cooling of the fluid in a physically constrained environment at elevated pressure*. Vapour-like magmatic fluids of low to moderate salinity can cool and contract to an aqueous liquid without heterogeneous phase transition, provided that pressure remains sufficiently high to prevent breaching of the two-phase field below ~450°C. Initial fluid cooling at elevated pressure may be realised near the brittle-to-ductile transition (Fournier 1987) in a near-neutral to mildly extensional crustal stress regime, which favours the emplacement of magma chambers without volcanic eruption and low-density vapour ejection to the surface (Tosdal and Richards 2001). Vapour contraction to aqueous liquid can be realised after single-phase fluid exsolution from the magma, or by hydrological conditions in which vapour physically separates from a hypersaline liquid (Fig. 3). The two alternative processes for generating low-salinity to medium-salinity epithermal liquids require similar geological conditions and are not easily discriminated using geological observations at the site of epithermal ore deposition, although inclusion evidence of intermittent entrainment of hypersaline liquid in epithermal deposits (Fig. 2) may be diagnostic for two-phase coexistence at depth.
2. *Initial excess of H_2S over Fe + Cu in the high-temperature fluid* is the foremost chemical requirement for efficient gold transport down to epithermal temperatures. The stoichiometric concentrations of total reduced sulphur (H_2S, HS^-) relative to those of metals saturating as sulphides at high temperature (Cu and Fe as $CuFeS_2$, Cu_5FeS_4, and FeS_2) constitute a *chemical divide*, across which, even small compositional variations lead to drastically different pathways of chemical-fluid evolution. Metal excess leads to sulphide depletion and rapid loss of gold solubility with falling temperature, whereas an initial H_2S excess can allow high gold solubilities, as bisulphide complexes, down to very low temperatures. Unusually low Cl/OH in the magma could generate single-phase low-salinity fluids with initial $FeCl_2 < H_2S$. For typical calc-alkaline magmas, separation of hypersaline liquid from vapour at high temperature is likely to have a decisive effect, because iron preferentially partitions into hypersaline liquid, while volatile sulphur species fractionate into the vapour. The source process for epithermal ore fluids is further optimised, where Cu, As and, especially, Au partition most strongly into the lower-salinity vapour, but these conditions are not yet well constrained by experiment.
3. *Acid neutralisation by wall rock reactions during fluid cooling* further optimises the likelihood that an initially H_2S, SO_2 and Au-rich fluid derived from magmatic vapour can carry its gold all the way to the site of epithermal ore formation. During fluid cooling in contact with intermediate-composition magmatic rocks, de-sulphidation of the fluid by iron in the wall rocks competes with the H^+ neutralising effect of feldspar-destructive alteration. As a result, cooling of a poorly focussed fluid in contact with an excess of magmatic rock would lead to variable amounts of potassic or propylitic alteration, and fixation of any gold in dispersed form. More favourable chemical evolution paths for effective gold transport are realised within zones of pervasive muscovite–pyrite alteration (± clay minerals ± sulphate ± carbonate),

permitting mildly acidic conditions without complete loss of H_2S. Such feldspar-destructive alteration zones (with pyrite but no remaining iron oxide or ferrous silicate near the central channelway) are widespread in the upper parts of porphyry-type deposits and are the most favourable ascent paths for gold from the site of vapour separation to the site of epithermal ore formation. Cross-cutting relationships seen in most porphyry deposits and the typical paragenetic sequence of high-sulphidation epithermal deposits are explained by gradual retraction of isotherms as the entire magmatic system cools, establishing a region of coexisting vapour + hypersaline liquid during continued fluid exsolution from a deeper magma chamber.

4. *Gold precipitation driven by a high degree of chemical disequilibrium* is the final requirement for efficient epithermal ore formation, by a variety of mechanisms imposing a localised drop in gold solubility. Possibilities include sulphide loss to a low-density steam phase (e.g. Drummond and Ohmoto 1985; Krupp and Seward 1987), mixing with groundwater (Stoffregen 1987; Spycher and Reed 1989; Mancano and Campbell 1995; Rohrlach 2003), or desulphidation driven by renewed reaction with fresh Fe-bearing igneous rocks or with diagenetic Fe carbonates in reduced sedimentary rocks (Muntean et al. 1990; Kettler et al. 1992; Kesler et al. 2003a). Modelling gold precipitation is not the aim of this paper, but any of the previously identified processes will lead to a higher-grade deposit, if the initial input fluid contains parts-per-million rather than parts-per-billion levels of gold.

In summary, this thermodynamic study explains how high-sulphidation epithermal and porphyry-style Cu–As–Au ore formation can be linked by the processes of phase separation between hypersaline liquids and vapour at high temperature, and subsequent cooling and contraction of the vapour to a low-salinity to intermediate-salinity liquid. Both mineralisation processes share a common fluid source, even when only one of them may generate economic ore in a particular system—a large intrusion of volatile-rich magma, from which magmatic–hydrothermal fluid is expelled against the load of overlying rocks in a partially confined upper-crustal plutonic regime. Fluid-phase separation at elevated pressure (>500 bar) and temperature (>500°C) affects initial ore metal partitioning but, more importantly, leads to partial segregation of sulphide required for gold complexing in vapour-derived low-salinity to intermediate-salinity fluids, from iron remaining preferentially in the hypersaline liquid. Excess sulphide over chalcophile metals enables transport of ppm-level concentrations of gold down to epithermal temperatures. Advanced argillic alteration followed by later pyrite–enargite–gold deposition in high-sulphidation epithermal deposits, and upward-flaring phyllic alteration zones overprinting subjacent porphyry-style ore deposits, are a common consequence of magmatic–hydrothermal systems in which fluids emanate from a successively downward-retracting magma front. Epithermal gold deposits of lower sulphidation state, while containing a greater proportion of meteoric water in veins that are more open to the hydrosphere, may also derive a dominant fraction of their gold endowment from a volumetrically minor fraction of magmatic vapour-derived fluid.

Acknowledgements This study builds on a long collaboration in the fluids and ore deposits group at ETH Zürich, which included Andreas Audétat, Thomas Driesner, Sebastian Geiger, Detlef Günther, Werner Halter, Kalin Kouzmanov, Marianne Landtwing, Thomas Pettke, Thomas Ulrich and others over the years. I am grateful for the thoughtful comments from Paul Barton, Lluis Fontboté, Steve Kesler, Robert Moritz, John Ridley, Mike Solomon, Noel White, Anthony Williams-Jones and other colleagues participating in the 2004 Swiss–Japanese Workshop on Epithermal Ore Deposits. Many thanks especially to Jeff Hedenquist and Hans Keppler who helped with careful reviews of the text. Research supported by ETH Zürich and the Swiss National Science Foundation (grants 20-59544-99 and 200020-100735).

References

Akinfiev NN, Zotov AV (2001) Thermodynamic description of chloride, hydrosulfide, and hydroxo complexes of Ag(I), Cu(I), and Au(I) at temperatures of 25–500°C and pressures of 1–2000 bar. Geochem Int 39(10):990–1006

Alderton DHM, Fallick AE (2000) The nature and genesis of gold–silver–tellurium mineralization in the Metaliferi Mountains of western Romania. Econ Geol 95(3):495–515

Anderko A, Pitzer KS (1993a) Equation-of-state representation of phase-equilibria and volumetric properties of the system NaCl–H_2O above 573 K. Geochim Cosmochim Acta 57(8):1657–1680

Anderko A, Pitzer KS (1993b) Phase-equilibria and volumetric properties of the systems KCl–H_2O and NaCl–KCl–H_2O above 573 K—equation of state representation. Geochim Cosmochim Acta 57(20):4885–4897

Arribas AJ (1995) Characteristics of high-sulfidation epithermal deposits, and their relation to magmatic fluid. In: Thompson JFH (ed) Magmas, fluids, and ore deposits. Mineralogical Association of Canada, pp 419–454

Arribas A, Cunningham CG, Rytuba JJ, Rye RO, Kelly WC, Podwysocki MH, McKee EH, Tosdal RM (1995a) Geology, geochronology, fluid inclusions, and isotope geochemistry of the Rodalquilar gold alunite deposit, Spain. Econ Geol Bull Soc Econ Geol 90(4):795–822

Arribas A, Hedenquist JW, Itaya T, Okada T, Concepcion RA, Garcia JS (1995b) Contemporaneous formation of adjacent porphyry and epithermal Cu–Au deposits over 300 ka in Northern Luzon, Philippines. Geology 23(4):337–340

Audétat A, Pettke T (2003) The magmatic–hydrothermal evolution of two barren granites: a melt and fluid inclusion study of the Rito del Medio and Canada Pinabete plutons in northern New Mexico (USA). Geochim Cosmochim Acta 67(1):97–121

Audétat A, Günther D, Heinrich CA (1998) Formation of a magmatic–hydrothermal ore deposit: insights with LA–ICP–MS analysis of fluid inclusions. Science 279(5359):2091–2094

Audétat A, Günther D, Heinrich CA (2000) Causes for large-scale metal zonation around mineralized plutons: fluid inclusion LA–ICP–MS evidence from the Mole Granite, Australia. Econ Geol 95(8):1563–1581

Audétat A, Pettke T, Dolejs D, Bodnar R (2002) Magmatic anhydrite in the Cu-porphyry-related magma at Santa Rita, New Mexico (USA). Geochim Cosmochim Acta 66:A37–A37

Bendezu R, Fontbote L, Cosca M (2003) Relative age of Cordilleran base metal lode and replacement deposits, and high sulfidation Au–(Ag) epithermal mineralization in the Colquijirca mining district, central Peru. Mineralium Deposita 38(6):683–694

Berger BR, Henley RW (1989) Advances in the understanding of epithermal gold–silver deposits, with special reference to the Western United States. In: Keays RR, Ramsay WHR, Groves DI (eds) The geology of gold deposits: The perspective in 1988. Economic Geology Monograph Series, pp 405–423

Bodnar RJ (1995) Fluid-inclusion evidence for a magmatic source for metals in porphyry copper deposits. In: Thompson EJFH (ed) Magmas, fluids and ore deposits. Mineralogical Association of Canada, Short Course Series, pp 139–152

Bodnar RJ, Vityk MO (1994) Interpretation of microthermometric data for H_2O–NaCl fluid inclusions. In: DeVivo, Frezzotti (eds) Fluid inclusions in minerals, pp 117–130

Bodnar RJ, Burnham CW, Sterner SM (1985) Synthetic fluid inclusions in natural quartz III determination of phase equilibrium properties in the system H_2O–NaCl to 1000°C and 1500 bars. Geochim Cosmochim Acta 49:1861–1873

Brimhall GH, Ghiorso MS (1983) Origin and ore-forming consequences of the advanced argillic alteration process in hypogene environments by magmatic gas contamination of meteoric fluids. Econ Geol 78(1):73–90

Burnham CW (1979) Magmas and hydrothermal fluids. In: Barnes HL (ed) Geochemistry of hydrothermal ore deposits, 2nd edn. Wiley, New York, pp 71–136

Burnham CW (1997) Magmas and hydrothermal fluids. In: Barnes HL (ed) Geochemistry of hydrothermal ore deposits, 3 edn. Wiley, New York, pp 63–125

Burnham CW, Ohmoto H (1980) Late-stage processes of felsic magmatism. Mining Geol Spec Issue 8:1–11

Cail TL, Cline JS (2001) Alteration associated with gold deposition at the Getchell Carlin-type gold deposit, north-central Nevada. Econ Geol 96(6):1343–1359

Camus F, Dilles JH (2001) A special issue devoted to porphyry copper deposits of northern Chile-Preface. Econ Geol 96(2):233–237

Candela PA (1989) Magmatic ore-forming fluids; thermodynamic and mass transfer calculations of metal concentrations. In: Whitney JA, Naldrett AJ (eds) Ore deposition associated with magmas. Reviews in Economic Geology. Society of Economic Geologists, Socorro, pp 203–221

Candela PA, Piccoli PM (1995) Model ore–metal partitioning from melts into vapor and vapor/brine mixtures. In: Thompson JFH (ed) Magmas, fluids and ore deposits. Mineralogical Association of Canada, pp 101–127

Carroll MR, Rutherford MJ (1987) The stability of igneous anhydrite—experimental results and implications for sulfur behavior in the 1982 El-Chichon trachyandesite and other evolved magmas. J Petrol 28(5):781–801

Carroll MR, Webster JD (1994) Solubilities of sulfur, noble gases, nitrogen, chlorine, and fluorine in magmas, volatiles in magmas. Reviews in Mineralogy, pp 231–279

Chou IM, Eugster HP (1977) Solubility of magnetite in supercritical chloride solutions. Am J Sci 277:1296–1314

Claveria RJR (2001) Mineral paragenesis of the Lepanto copper and gold and the Victoria gold deposits, Mankayan Mineral District, Philippines. Resource Geol 51(2):97–106

Cline JS, Bodnar RJ (1991) Can economic porphyry copper mineralization be generated by a typical calc-alkaline melt? J Geophys Res 96:8113–8126

Cline JS, Bodnar RJ (1994) Direct evolution of brine from a crystallizing silicic melt at the Questa, New Mexico, molybdenum deposit. Econ Geol 89:1780–1802

Cline JS, Hofstra AA (2000) Ore–fluid evolution at the Getchell Carlin-type gold deposit, Nevada, USA. Eur J Mineral 12(1):195–212

Core D, Kesler SE, Essene EJ, Campbell IH, Allen CM (2004) Copper-rich source regions for giant porphyry copper deposits: Last Chance Stock, Bingham, Utah, SEG Conference on Predictive Mineral Discovery Under Cover: Perth, Australia, pp 230–233

Craig JR, Barton PB (1973) Thermochemical approximations for sulfosalts. Econ Geol 68(4):493–506

Delmelle P, Bernard A (1994) Geochemistry, mineralogy, and chemical modeling of the acid crater lake of Kawah Ijen Volcano, Indonesia. Geochim Cosmochim Acta 58(11):2445–2460

Ding K, Seyfried WE (1992) Determination of Fe–Cl complexing in the low-pressure supercritical region (NaCl fluid)—iron solubility constraints on pH of subseafloor hydrothermal fluids. Geochim Cosmochim Acta 56(10):3681–3692

Driesner T (2001) A new model for the thermodynamic and transport properties of the NaCl–Water System from 0–700°C, 0.1 to 500 MPa, and X_{NaCl} from 0 to 1. 11th Annual Goldschmidt Conference, Hot Springs, Virginia

Driesner T, Heinrich CA (2002) Revised critical curve for the system H_2O–NaCl 12th Annual Goldschmidt Conference, Davos. Geochim Cosmochim Acta A196

Drummond SE, Ohmoto H (1985) Chemical evolution and mineral deposition in boiling hydrothermal systems. Econ Geol 80(1):126–147

Eastoe CJ (1978) Fluid inclusion study of Panguna–porphyry–copper deposit, Bougainville, Papua, New Guinea. Econ Geol 73(5):721–748

Eastoe CJ (1982) Physics and chemistry of the hydrothermal system at the Panguna porphyry copper deposit, Bougainville, Papua, New Guinea. Econ Geol 77(1):127–153

Einaudi MT, Hedenquist JW, Inan EE (2003) Sulfidation state of fluids in active and extinct hydrothermal systems: transitions from porphyry to epithermal environments. In: Simmons SF, Graham I (eds) Volcanic, geothermal and ore-forming fluids: Rulers and witnesses of processes within the earth. Econ Geol Spec Publ 343

Emsbo P, Hofstra AH, Lauha EA, Griffin GL, Hutchinson RW (2003) Origin of high-grade gold ore, source of ore fluid components, and genesis of the Meikle and neighboring Carlin-type deposits, northern Carlin trend, Nevada. Econ Geol 98(6):1069–1105

Etminan H (1977) Le porphyre cuprifère de Sar Cheshmeh (Iran); rôle des phases fluides dans les mècanismes dàltèration et de minèralisation. PhD Thesis, Mem Sci Terre Universitè Nancy (France) 34:249

Fournier RO (1987) Conceptual models of brine evolution in magmatic–hydrothermal systems. In: Decker RW, Wright TL, Stauffer PH (eds) Volcanism in Hawaii. Hawaiian Volcano Observatory, pp 1487–1506

Fournier RO (1999) Hydrothermal processes related to movement of fluid from plastic into brittle rock in the magmatic–epithermal environment. Econ Geol 94:1193–1211

Frank MR, Candela PA, Piccoli PM, Glascock MD (2002) Gold solubility, speciation, and partitioning as a function of HCl in the brine–silicate melt–metallic gold system at 800°C and 100 MPa. Geochim Cosmochim Acta 66(21):3719–3732

Frank MR, Candela PA, Piccoli PM (2003) Alkali exchange equilibria between a silicate melt and coexisting magmatic volatile phase: an experimental study at 800°C and 100 MPa. Geochim Cosmochim Acta 67(7):1415–1427

Gammons CH, Williams-Jones AE (1997) Chemical mobility of gold in the porphyry–epithermal environment. Econ Geol 92(1):45–59

Giggenbach WF (1980) Geothermal gas equilibria. Geochim Cosmochim Acta 44(12):2021–2032

Giggenbach WF (1992) SEG distinguished lecture—magma degassing and mineral deposition in hydrothermal systems along convergent plate boundaries. Econ Geol 87(7):1927–1944

Gustafson LB, Hunt JP (1975) Porphyry copper deposit at El Salvador, Chile. Econ Geol 70(5):857–912

Halter WE, Pettke T, Heinrich CA (2002) The origin of Cu/Au ratios in porphyry-type ore deposits. Science 296(5574):1844–1846

Halter WE, Pettke T, Heinrich CA (2004) Magma evolution and the formation of porphyry Cu–Au ore fluids: evidence from silicate and sulfide melt inclusions. Mineralium Deposita (in press)

Hattori KH, Keith JD (2001) Contribution of mafic melt to porphyry copper mineralization: evidence from Mount Pinatubo, Philippines, and Bingham Canyon, Utah, USA. Mineralium Deposita 36(8):799–806

Heald P, Foley NK, Hayba DO (1987) Comparative anatomy of volcanic-hosted epithermal deposits—acid sulfate and Adularia–sericite types. Econ Geol 82(1):1–26

Hedenquist JW, Lowenstern JB (1994) The role of magmas in the formation of hydrothermal ore deposits. Nature 370(6490):519–527

Hedenquist JW, Richards JP (1998) The influence of geochemical techniques on the development of genetic models for porphyry copper deposits. In: Richards JP, Larson PB (eds) Techniques in hydrothermal ore deposits geology. Reviews in Economic Geology, pp 235–256

Hedenquist JW, Simmons SF, Giggenbach WF, Eldridge CS (1993) White-Island, New Zealand, volcanic–hydrothermal system represents the geochemical environment of high-sulfidation Cu and Au ore deposition. Geology 21(8):731–734

Hedenquist JW, Aoki M, Shinohara H (1994a) Flux of volatiles and ore-forming metals from the magmatic–hydrothermal system of Satsuma Iwojima Volcano. Geology 22(7):585–588

Hedenquist JW, Matsuhisa Y, Izawa E, White NC, Giggenbach WF, Aoki M (1994b) Geology, geochemistry, and origin of high sulfidation Cu–Au mineralization in the Nansatsu district, Japan. Econ Geol 89(1):1–30

Hedenquist JW, Arribas A, Reynolds TJ (1998) Evolution of an intrusion-centered hydrothermal system: far Southeast-Lepanto porphyry and epithermal Cu–Au deposits, Philippines. Econ Geol 93(4):373–404

Heinrich CA, Eadington PJ (1986) Thermodynamic predictions of the hydrothermal chemistry of arsenic, and their significance for the paragenetic sequence of some cassiterite–arsenopyrite–base metal sulfide deposits. Econ Geol 81(3):511–529

Heinrich CA, Ryan CG, Mernagh TP, Eadington PJ (1992) Segregation of ore metals between magmatic brine and vapor—a fluid inclusion study using pixe microanalysis. Econ Geol 87(6):1566–1583

Heinrich CA, Walshe JL, Harrold BP (1996) Chemical mass transfer modelling of ore-forming hydrothermal systems: current practise and problems. Ore Geol Rev 10(3-6):319–338

Heinrich CA, Günther D, Audétat A, Ulrich T, Frischknecht R (1999) Metal fractionation between magmatic brine and vapor, determined by microanalysis of fluid inclusions. Geology 27(8):755–758

Heinrich CA, Pettke T, Halter WE, Aigner-Torres M, Audétat A, Günther D, Hattendorf B, Bleiner D, Guillong M, Horn I (2003) Quantitative multi-element analysis of minerals, fluid and melt inclusions by laser-ablation inductively-coupled-plasma mass spectrometry. Geochim Cosmochim Acta 67(18):3473–3497

Heinrich CA, Driesner T, Stefansson A, Seward TM (2004) Magmatic vapor contraction and the transport of gold from porphyry to epithermal ore deposits. Geology 32(9):761–764

Helgeson HC (1970) A chemical and thermodynamic model of ore deposition in hydrothermal systems. Mineral Soc Am Spec Paper 3:155–186

Hemley JJ, Cygan GL, Fein JB, Robinson GR, D'Angelo WM (1992) Hydrothermal ore-forming processes in the light of studies in rock-buffered systems 1 Iron–copper–zinc–lead sulfide solubility relations. Econ Geol 87(1):1–22

Henley RW, McNabb A (1978) Magmatic vapor plumes and ground–water interaction in porphyry copper emplacement. Econ Geol 73:1–20

Ho PC, Palmer DA, Gruszkiewicz MS (2001) Conductivity measurements of dilute aqueous HCl solutions to high temperatures and pressures using a flow-through cell. J Phys Chem B 105(6):1260–1266

Holland TJB, Powell R (1998) An internally consistent thermodynamic data set for phases of petrological interest. J Metamorp Geol 16(3):309–343

Iakovleva VP (2003) UV specrophotometric studies of arsenic(III) and antimony(IIII) aqueous chemistry from 25 to 300°C. Unpubl PhD Thesis, ETH Zürich

Jannas RR, Beane RE, Ahler BA, Brosnahan DR (1990) Gold and copper mineralization at the El-Indio deposit, Chile. J Geochem Exploration 36(1-3):233–266

Johnson JW, Oelkers EH, Helgeson HC (1992) SUPCTR92—a software package for calculating the standard molal thermodynamic properties of minerals, gases, aqueous species, and reactions from 1 bar to 5000 bar and 0°C to 1000°C. Comput Geosci 18(7):899–947

Johnston MK, Ressel MW (2004) Carlin-type and distal-disseminated Au–Ag deposits: related distal expressions of Eocene intrusive centers in North-Central Nevada. SEG Newslett 59:12–14

Kehayov R, Bogdanov K, Fanger L, von Quadt A, Pettke T, Heinrich CA (2003) The fluid chemical evolution of the Elatiste porphyry Cu–Au–PGE deposit, Bulgaria. In: Eliopoulos DG (ed) Mineral exploration and sustainable development. Millpress, Rotterdam, pp 1173–1176

Keppler H (1999) Experimental evidence for the source of excess sulfur in explosive volcanic eruptions. Science 284:1652–1654

Kesler SE, Ye Z, Fortuna J, Riciputi LC (2003b) Epithermal–Carlin transition: evidence for magmatic input into Carlin-type deposits. In: Eliopoulos DG (ed) Mineral exploration and sustainable development. Millpress, Rotterdam, pp 493–494

Kesler SE, Fortuna J, Ye ZJ, Alt JC, Core DP, Zohar P, Borhauer J, Chryssoulis SL (2003a) Evaluation of the role of sulfidation in deposition of gold, Screamer section of the Betze–Post Carlin-type deposit, Nevada. Econ Geol 98(6):1137–1157

Kettler RM, Rye RO, Kessler SE, Meyers PA, Polanco J, Russell N (1992) Gold deposition by sulfidation of ferrous Fe in the Lacustrine sediments of the Pueblo Viejo district (Dominican Republic)—the effect of Fe–C–S diagenesis on later hydrothermal mineralization in a maar diatreme complex. Chem Geol 99(1–3):29–50

Kouzmanov K, Ramboz C, Lerouge C, Deloule E, Beaufort D, Bogdanov K (2003) Stable isotopic constraints on the origin of epithermal Cu–Au and related porphyry copper mineralisations in the southern Pangyurishte district, Srednogorie zone, Bulgaria. In: Eliopoulos DG (ed) Mineral exploration and sustainable development. Millpress, Rotterdam, pp 1181–1184

Krupp RE, Seward TM (1987) The Rotokawa geothermal system, New Zealand—an active epithermal gold-depositing environment. Econ Geol 82(5):1109–1129

Landtwing MR, Pettke T, Halter WE, Heinrich CA, Redmond PB, Einaudi MT (2004) Causes for Cu–Fe–sulfide deposition in the Bingham porphyry Cu–Au–Mo deposit, Utah: combined SEM-cathodoluminescence petrography and LA–ICPMS analysis of fluid inclusions. Earth Planetary Sci Lett (in press)

Liu WH, McPhail DC, Brugger J (2001) An experimental study of copper(I) chloride and copper(I) acetate complexing in hydrothermal solutions between 50°C and 250°C and vapor-saturated pressure. Geochim Cosmochim Acta 65(17):2937–2948

Losada-Calderòn AJ, McPhail DC (1996) Porphyry and high-sulfidation epithermal mineralization in the Nevados del Famatina mining district, Argentina. In: Camus F, Sillitoe RM, Peterson R (eds) Andean copper deposits: new discoveries, mineralization, styles and metallogeny. Soc Econ Geol Spec Publ 5:91–118

Loucks RR, Mavrogenes JA (1999) Gold solubility in supercritical hydrothermal brines measured in synthetic fluid inclusions. Science 284(5423):2159–2163

Luhr JF (1990) Experimental phase-relations of water-saturated and sulfur-saturated arc magmas and the 1982 eruptions of El-Chichon volcano. J Petrol 31(5):1071–1114

Mancano DP, Campbell AR (1995) Microthermometry of enargite-hosted fluid inclusions from the Lepanto, Philippines, high-sulfidation Cu–Au deposit. Geochim Cosmochim Acta 59(19):3909–3916

Moritz R, Jacquat S, Chambefort I, Fontignie D, Petrunov R, Georgieva S, von Quadt A (2003) Controls on ore formation at the high-sulfidation Au–Cu Chelopech deposit, Bulgaria: evidence from infrared fluid inclusion microthermometry of enargite and isotope systematics of barite. In: Eliopoulos DG (ed) Mineral exploration and sustainable development. Millpress, Rotterdam, pp 1209–1212

Mountain BW, Seward TM (1999) The hydrosulfide sulfide complexes of copper(I): experimental determination of stoichiometry and stability at 22°C and reassessment of high temperature data. Geochim Cosmochim Acta 63(1):11–29

Muntean JL, Einaudi MT (2001) Porphyry–epithermal transition: Maricunga belt, northern Chile. Econ Geol 96(4):743–772

Muntean JL, Kesler SE, Russell N, Polanco J (1990) Evolution of the Monte Negro acid sulfate Au–Ag deposit, Pueblo Viejo, Dominican Republic—important factors in grade development. Econ Geol 85(8):1738–1758

Oelkers EH, Helgeson HC (1991) Calculation of activity coefficients and degrees of formation of neutral ion-pairs in supercritical electrolyte solutions. Geochim Cosmochim Acta 55(5):1235–1251

Perello J, Cox D, Garamjav D, Sanjdorj S, Diakov S, Schissel D, Munkhbat TO, Oyun G (2001) Oyu Tolgoi, Mongolia: Siluro–Devonian porphyry Cu–Au–(Mo) and high-sulfidation Cu mineralization with a cretaceous chalcocite blanket. Econ Geol 96(6):1407–1428

Pokrovski G, Gout R, Schott J, Zotov A, Harrichoury JC (1996) Thermodynamic properties and stoichiometry of As(III) hydroxide complexes at hydrothermal conditions. Geochim Cosmochim Acta 60(5):737–749

Rankin AH, Ramsey MH, Coles B, Vanlangevelde F, Thomas CR (1992) The composition of hypersaline, iron-rich granitic fluids based on laser-ICP and Synchrotron-XRF microprobe analysis of individual fluid inclusions in Topaz, Mole Granite, Eastern Australia. Geochim Cosmochim Acta 56(1):67–79

Ransome FL (1907) The association of alunite with gold in the Goldfield district, Nevada. Econ Geol 2:667–692

Redmond PB, Einaudi MT, Inan EE, Landtwing MR, Heinrich CA (2004) Copper deposition by fluid cooling in intrusion-centered systems: new insights from the Bingham porphyry ore deposit, Utah. Geology 32(3):217–220

Reynolds TJ, Beane RE (1985) Evolution of hydrothermal fluid characteristics at the Santa Rita, New Mexico, porphyry copper deposit. Econ Geol 80:1328–1347

Richards JP, Bray CJ, Channer DMD, Spooner ETC (1997) Fluid chemistry and processes at the Porgera gold deposit, Papua New Guinea. Mineralium Deposita 32(2):119–132

Roedder E (1971) Fluid inclusion studies on the porphyry-type ore deposits at Bingham, Utah, Butte, Montana, and Climax, Colorado. Econ Geol 66(1):98–118

Rohrlach BD (2003) Tectonic evolution, petrochemistry, geochronology and palaeohydrology of the Tampakan Porphyry and high-sulfidation epithermal Cu–Au deposit, Mindanao, Philippines. unpubl PhD Thesis, Australian National University, pp 499, 23 app

Ronacher E, Richards JP, Reed MH, Bray CJ, Spooner ETC, Adams PD (2004) Characteristics and evolution of the hydrothermal fluid in the North zone high-grade area, Porgera gold deposit, Papua New Guinea. Econ Geol 99(5):843–867

Ruggieri G, Lattanzi P, Luxoro SS, Dessi R, Benvenuti M, Tanelli G (1997) Geology, mineralogy, and fluid inclusion data of the Furtei high-sulfidation gold deposit, Sardinia, Italy. Econ Geol 92(1):1–19

Rusk B, Reed MH, Dilles JH, Klemm L (2004) Compositions of magmatic–hydrothermal fluids determined by LA–ICPMS of fluid inclusions from the porphyry copper–molybdenum deposit at Butte, Montana. Chem Geol 210(1-4):173–199

Rye RO (1993) The evolution of magmatic fluids in the epithermal environment—the stable isotope perspective. Econ Geol 88(3):733–753

Sänger von Oepen P, Friedrich G, Vogt JH (1989) Fluid evolution, wall rock alteration, and ore mineralization associated with the Rodalquilar epithermal gold deposit in Southeast Spain. Mineralium Deposita 24(4):235–243

Sawkins FJ (1990) Metal deposits in relation to plate tectonics. Minerals and Rocks, 17. Springer, Berlin Heidelberg New York, p 461

Sawkins FJ, Scherkenbach DA (1981) High copper content of fluid inclusions in quartz from northern Sonora: implications for ore genesis theory. Geology 9:37–40

Seal RR, Essene EJ, Kelly WC (1990) Tetrahedrite and tennantite—evaluation of thermodynamic data and phase equilibria. Can Mineral 28:725–738

Shinohara H, Hedenquist JW (1997) Constraints on magma degassing beneath the far southeast porphyry Cu–Au deposit, Philippines. J Petrol 38(12):1741–1752

Shinohara H, Kazahaya K, Lowenstern JB (1995) Volatile transport in a convecting magma column—implications for porphyry Mo mineralization. Geology 23(12):1091–1094

Sillitoe RH (1973) The tops and bottoms of porphyry copper deposits. Econ Geol 68(6):799–815

Sillitoe RH (1983) Enargite-bearing massive sulfide deposits high in porphyry copper systems. Econ Geol 78(2):348–352

Sillitoe RH (1994) Erosion and collapse of volcanoes—causes of telescoping in intrusion-centered ore deposits. Geology 22(10):945–948

Sillitoe RH (1997) Characteristics and controls of the largest porphyry copper–gold and epithermal gold deposits in the circum-Pacific region. Austral J Earth Sci 44(3):373–388

Sillitoe RH, Bonham HF (1990) Sediment-hosted gold deposits—distal products of magmatic–hydrothermal systems. Geology 18(2):157–161

Sillitoe RH, Hedenquist JW (2003) Linkages between volcanotectonic settings, ore-fluid compositions and epithermal precious metal deposits. In: Simmons SF, Graham I (eds) Volcanic, geothermal and ore-forming fluids: rulers and witnesses of processes within the earth. Econ Geol Spec Publ 343

Solomon M (1990) Subduction, arc reversal, and the origin of porphyry copper–gold deposits in island arcs. Geology 18:630–633

Spycher NF, Reed MH (1989) Evolution of a broadlands-type epithermal ore fluid along alternative *P*–*T*paths—implications for the transport and deposition of base, precious, and volatile metals. Econ Geol 84(2):328–359

Stefánsson A (2003) The stability and stoichiometry of gold(I) and silver(I) complexes in hydrothermal solutions. PhD Thesis 14808, ETH Zürich, 142 pp, 2 Appendices

Stefánsson A, Seward TM (2003) Stability of chloridogold(I) complexes in aqueous solutions from 300 to 600°C and from 500 to 1800 bar. Geochim Cosmochim Acta 67(23):4559–4576

Stefánsson A, Seward TM (2004) Gold(I) complexing in aqueous sulfide solutions to 500°C at 500 bar. Geochim Cosmochim Acta 68:4121–4143

Stoffregen R (1987) Genesis of acid-sulfate alteration and Au–Cu–Ag mineralization at Summitville, Colorado. Econ Geol 82(6):1575–1591

Stoffregen RE, Alpers CN, Jambor JL (2000) Alunite–jarosite crystallography, thermodynamics, and geochronology: sulfate minerals—crystallography, geochemistry and environmental significance. Mineral Soc Am Rev Mineral 40:453–479

Streck MJ, Dilles JH (1998) Sulfur evolution of oxidized arc magmas as recorded in apatite from a porphyry copper batholith. Geology 26(6):523–526

Sverjensky DA, Shock EL, Helgeson HC (1997) Prediction of the thermodynamic properties of aqueous metal complexes to 1000°C and 5 kb. Geochim Cosmochim Acta 61(7):1359–1412

Symonds RB, Rose WI, Bluth GJS, Gerlach TM (1994) Volcanic gas studies—methods, results, and applications: volatiles in magmas. Reviews in Mineralogy, pp 1–66

Taran YA, Hedenquist JW, Korzhinsky MA, Tkachenko SI, Shmulovich KI (1995) Geochemistry of magmatic gases from Kudryavy Volcano, Iturup, Kuril Islands. Geochim Cosmochim Acta 59(9):1749–1761

Taylor HP (1974) Application of oxygen and hydrogen isotope studies to problems of hydrothermal alteration and ore deposition. Econ Geol 69(6):843–883

Tosdal RM, Richards JP (2001) Magmatic and structural controls on the development of porphyry Cu ± Mo ± Au deposits. In: Richards JP, Tosdal RM (eds) Structural controls on ore genesis. Reviews in Economic Geology, pp 157–180

Turnbull AG, Wadsley MW (1986) The CSIRO-SGTE THERMODATA System (Version V). Commonwealth Scientific and Industrial Research Organisation, Port Melbourne, Division of Mineral Chemistry Communications 1–7:413

Ulrich T, Heinrich CA (2001) Geology and alteration geochemistry of the porphyry Cu–Au deposit at Bajo de la Alumbrera, Argentina (2001) Economic Geology 96:1719, correctly reprinted in 2002 97(8):1863–1888

Ulrich T, Günther D, Heinrich CA (1999) Gold concentrations of magmatic brines and the metal budget of porphyry copper deposits. Nature 399:676–679

Ulrich T, Günther D, Heinrich CA (2001) Evolution of a porphyry Cu–Au deposit, based on LA–ICP-MS analysis of fluid inclusions: Bajo de la Alumbrera, Argentina. Economic Geology 96:1743, correctly reprinted in 2002 97(8):1888–1920

Vennemann TW, Muntean JL, Kesler SE, Oneil JR, Valley JW, Russell N (1993) Stable isotope evidence for magmatic fluids in the Pueblo-Viejo epithermal acid sulfate Au–Ag deposit, Dominican Republic. Econ Geol 88(1):55–71

Wang Y, Sasaki M, Sasada M, Chen C-H (1999) Fluid inclusion studies of the Chinkuashih high-sulfidation gold–copper deposits in Taiwan. Chem Geol 154:155–167

Watanabe Y, Hedenquist J (2001) Mineralogic and stable isotope zonation at the surface over the El Salvador porphyry copper deposit, Chile. Econ Geol 96(8):1775–1797

Webster JG (1990) The solubility of As_2S_3 and speciation of As in dilute and sulfide-bearing fluids at 25 and 90°C. Geochim Cosmochim Acta 54(4):1009–1017

White NC, Hedenquist JW (1990) Epithermal environments and styles of mineralization—variations and their causes, and guidelines for exploration. J Geochem Exploration 36(1-3):445–474

Williams TJ, Candela PA, Piccoli PM (1997) Hydrogen–alkali exchange between silicate melts and two-phase aqueous mixtures: an experimental investigation. Contrib Mineral Petrol 128(2-3):114–126

Williams PJ, Bin Fu, Pollard PJ, Baker T, Margotomo W, Ryan CG, Van Achterbergh E, Mernagh TP, Condliffe E, Yardley BWD (2003) Fluid inclusion geochemistry of the Grasberg Cu–Au porphyry (abstract). Appl Earth Sci Trans Inst Min Metall B112

Williams-Jones AE, Migdisov AA, Archibald SM, Xiao ZF (2002) Vapor-transport of ore metals. In: Hellmann R, Wood SA (eds) Water–rock interaction: a tribute to David A Crerar. The Geochemical Society, Special Publication, pp 279–305

Wilson JWJ, Kesler SE, Cloke PL, Kelly WC (1980) Fluid inclusion geochemistry of the Granisle and Bell porphyry copper deposits, British Columbia. Econ Geol 75(1):45–61

Woitsekhowskaya MB, Peters SG (1998) Geochemical modeling of alteration and gold deposition at the Betze deposit, Eureka County, Nevada: U.S. Geological Survey Open File Report 98–338, 211–222

Xiao ZF, Gammons CH, Williams-Jones AE (1998) Experimental study of copper(I) chloride complexing in hydrothermal solutions at 40 to 300°C and saturated water vapor pressure. Geochim Cosmochim Acta 62(17):2949–2964

Zotov AV, Kudrin AV, Levin KA, Shilina ND, Var'yash LN (1995) Experimental studies of the solubility and complexing of selected ore elements (Au, Ag, Cu, Mo, As, Sb, Hg) in aqueous solution. In: Shmulovich KI, Yardley BWD, Gonchar GG (eds) Fluids in the crust. Chapman & Hall, London, pp 95–137